Mitofusins *Mfn1* and *Mfn2* are required to preserve glucose- but not incretin-stimulated beta cell connectivity and insulin secretion

Eleni Georgiadou[1], Charanya Muralidharan[2], Michelle Martinez[2], Pauline Chabosseau[1], Alejandra Tomas[1], Fiona Yong Su Wern[3], Elina Akalestou[1] Theodoros Stylianides[4], Asger Wretlind[5], Cristina Legido-Quigley[5,6], Ben Jones[7], Livia Lopez Noriega[1], Yanwen Xu[8], Guoqiang Gu[8], Nour Alsabeeh[9], Céline Cruciani-Guglielmacci[10], Christophe Magnan[10], Mark Ibberson[11], Isabelle Leclerc[1], Yusuf Ali[3], Scott A. Soleimanpour[12,13] Amelia K. Linnemann[2], Tristan A. Rodriguez[14] and Guy A. Rutter[1,3,15*].

[1]Section of Cell Biology and Functional Genomics, Division of Diabetes, Endocrinology and Metabolism, Department of Medicine, Imperial College London, London, W12 0NN, UK
[2]Center for Diabetes and Metabolic Diseases, Indiana University School of Medicine, Indianapolis, IN, 46202, USA
[3]Lee Kong Chian School of Medicine, Nanyang Technological University, 637553, Singapore
[4]Loughborough University, Centre of Innovative and Collaborative Construction Engineering, Leicestershire, LE11 3TU, UK
[5]Systems Medicin, Steno Diabetes Center Copenhagen, 2820, Denmark
[6] Institute of Pharmaceutical Science, Kings College London, London, SE1 9NH, UK
[7] Section of Endocrinology and Investigative Medicine, Imperial College London, W12 0NN,UK
[8]Department of Cell and Developmental Biology, Program of Developmental Biology, and Vanderbilt Center for Stem Cell Biology. Vanderbilt University, School of Medicine, Nashville, TN, 37232, USA.
[9]Kuwait University, Department of Physiology, Health Sciences Center, 13110, Kuwait
[10]Université de Paris, BFA, UMR 8251, CNRS, Regulation of Glycemia by Central Nervous System, Paris, 75205, France
[11]Vital-IT Group, SIB Swiss Institute of Bioinformatics, Lausanne, CH-1015, Switzerland
[12]Division of Metabolism, Endocrinology & Diabetes and Department of Internal Medicine, University of Michigan Medical School, Ann Arbor, MI 48105, USA
[13]VA Ann Arbor Healthcare System, Ann Arbor, MI 48105, USA
[14]National Heart and Lung Institute, Imperial Centre for Translational and Experimental Medicine, Imperial College London, London, W12 0NN, UK
[15] Centre of research of CHUM, University of Montreal, Quebec, H2X 0A9, Canada

*Address correspondence to Professor Guy A. Rutter, g.rutter@imperial.ac.uk, +44 20 759 43340

Word count: 4341

Abstract

Aims/hypothesis Mitochondrial glucose metabolism is essential for stimulated insulin release from pancreatic beta cells. Whether mitochondrial networks may be important for glucose or incretin sensing has yet to be determined.

Methods Here, we generated mice with beta cell-selective, adult-restricted deletion of the mitofusin genes *Mfn1* and *Mfn2* (β*Mfn1/2* dKO). Whole or dissociated pancreatic islets were used for live beta cell fluorescence imaging of cytosolic or mitochondrial Ca^{2+} concentration and ATP production or GSIS in response to increasing glucose concentrations or GLP-1 receptor agonists. Serum and blood samples were collected to examine oral and i.p. glucose tolerance.

Results β*Mfn1/2* dKO mice displayed elevated fed and fasted glycaemia ($p<0.01$, $p<0.001$) and a >five-fold decrease ($p<0.0001$) in plasma insulin. Mitochondrial length, glucose-induced polarisation, ATP synthesis and cytosolic Ca^{2+} increases were all reduced ($p<0.05$,$p<0.01$,$p<0.0001$) in dKO islets, and beta cell Ca^{2+} dynamics were suppressed *in vivo* ($p<0.001$). In contrast, oral glucose tolerance was near normal in β*Mfn1/2* dKO mice ($p<0.05$, $p<0.01$) and GLP-1 or GIP receptor agonists largely corrected defective GSIS from isolated islets through an EPAC-dependent signalling activation.

Conclusions/interpretation Mitochondrial fusion and fission cycles are thus essential in the beta cell to maintain normal glucose, but not incretin, sensing. Defects in these cycles in some forms of diabetes might therefore provide opportunities for novel incretin-based or other therapies.

Keywords: Ca^{2+} dynamics; exendin-4; glucose-stimulated insulin secretion; incretins; intercellular connectivity; mitochondrial dysfunction; mitofusins; pancreatic beta cell; Type 2 diabetes.

Graphical abstract

Figure legend

Impact of Mfn1/2 deletion on glucose and incretin stimulated-insulin secretion in beta cells. (A) In control animals, glucose is taken up by beta cells through GLUT2 and metabolised by mitochondria (elongated structure) through the citrate (TCA) cycle, leading to an increased mitochondrial proton motive force (hyperpolarised $\Delta\psi_m$), accelerated ATP synthesis and O_2 consumption rate (OCR). Consequently, the cytoplasmic ATP:ADP ratio rises, which causes closure of KATP channels, depolarisation of plasma membrane potential (ψm), opening of VDCCs and influx of cytosolic Ca^{2+}. Elevated $[Ca^{2+}]_{cyt}$ triggers a number of ATP-dependent processes including insulin secretion and improved beta-beta cell communication through connexin 36 (Cx36). (B) Following *Mfn1/2* deletion (β*Mfn1/2* dKO), highly fragmented mitochondria were associated with reduced mitochondrial Ca^{2+} ($[Ca^{2+}]_m$) accumulation, leading to a less polarised $\Delta\psi_m$, weaker OCR, lower mtDNA copy number and decreased ATP synthesis. This is expected to result in weaker ψm depolarisation, cytosolic Ca^{2+} influx and beta-beta cell connectivity due to lower expression of Cx36. Despite observing a higher number of docked insulin granules on the plasma membrane, insulin secretion was highly suppressed in these animals. This was also associated with increased beta cell death and reduced beta cell mass. (C) In response to incretins, insulin secretion is potentiated through the activation of GLP1-R and cAMP signalling involving PKA- and EPAC2-dependent pathways. Elevated $[Ca^{2+}]_{cyt}$ triggers a number of ATP-dependent processes including insulin secretion and Ca2+ removal into the endoplasmic reticulum (ER).(D) In β*Mfn1/2* dKO cells, activation of the GLP1-R was shown to be linked with a potentiation of the EPAC2 pathway that is PKA independent, along with an increased ER Ca^{2+} uptake and improved beta-beta cell communication. How these 'amplifying' signals of glucose metabolism for insulin secretion are linked with fragmented mitochondria remains unknown. Red and bold arrows represent enhanced pathways; dashed arrows represent impaired pathways. This figure was produced using illustrations from Servier Medical Art, http://smart.servier.com/

96 **List of abbreviations**

97 $[Ca^{2+}]_{cyt}$: Cytoplasmic Ca^{2+} concentration

98 $[Ca^{2+}]_{mito}$: Mitochondrial free Ca^{2+} concentration

99 AA: Antimycin A

100 Ach: Acetylcholine

101 *Clec16a*$^{\Delta panc}$: Pancreatic islet specific Clec16a knock-out

102 Diaz: Diazoxide

103 dKO: double knock-out

104 Ex4: Exendin-4

105 FCCP: Carbonyl cyanide-4-phenylhydrazone

106 GIP: Glucose-dependent insulinotropic peptide

107 GLP-1: Glucagon-like peptide-1

108 GSIS: Glucose-stimulated insulin secretion

109 IMM: Inner mitochondria membrane

110 IPGTT: Intraperitoneal glucose tolerance test

111 OGTT: Oral gavage and glucose tolerance test

112 Oligo: Oligomycin

113 OMM: Outer mitochondrial membrane

114 r: Pearson correlation coefficient

115 Rot: Rotenone

116 TMRE: Tetramethylrhodamine ethyl ester

117 β*Mfn1/2* dKO: beta cell specific Mitofusin 1 and 2 double knock-out

118 $\Delta\psi_m$: Mitochondrial membrane potential

Research in context

What is already known about this subject?

- Mitochondrial ultrastructural variations and number are altered in beta cells of human T2D patients [1].
- Mice lacking *Opa1*, which controls mitochondrial fusion and inner membrane cristae structure, in beta cells, develop hyperglycaemia and defects in GSIS [2].

What is the key question?

- Is an interconnected mitochondrial network essential in primary mouse beta cells for normal insulin secretion and glucose homeostasis?

What are the new findings?

- We generated mice with beta cell-selective, adult-restricted deletion of the mitofusin genes *Mfn1* and *Mfn2* and show that insulin secretion and glucose homeostasis are strongly reduced *in vivo*.
- Cytosolic and mitochondrial Ca^{2+} increases, $\Delta\psi_m$, ATP production and beta cell connectivity are impaired in β*Mfn1/2* dKO animals.
- Incretins bypass the above defects through an exchange protein directly activated by cAMP (EPAC)-dependent signalling mechanism.

How might this impact on clinical practice in the foreseeable future?

- The ability of incretins to bypass defects in mitochondrial function might be exploited by the design of new agonists which target this pathway.

139 **Introduction**

140 Mitochondria are often referred to as the powerhouses or “chief executive organelles”
141 of the cell, using fuels to provide most of the energy required to sustain normal function
142 [3]. Mitochondrial oxidative metabolism plays a pivotal role in the response of
143 pancreatic beta cells to stimulation by glucose and other nutrients [4]. Thus, as blood
144 glucose increases, enhanced glycolytic flux and oxidative metabolism lead to an
145 increase in ATP synthesis, initiating a cascade of events which involve the closure of
146 ATP-sensitive K^+ (K_{ATP}) channels [5], plasma membrane depolarisation and the influx
147 of Ca^{2+} via voltage-dependent Ca^{2+} channels (VDCC). The latter, along with other,
148 less well defined “amplifying” signals [6], drive the biphasic release of insulin [4]. Gut-
149 derived incretin hormones including glucagon-like peptide-1 (GLP-1) and glucose-
150 dependent insulinotropic peptide (GIP) [7] further potentiate secretion by binding to
151 class-B G-protein coupled receptors (GPCRs) to generate cAMP and other
152 intracellular signals [8].

153

154 Changes in mitochondrial function in beta cells may also contribute to declining insulin
155 secretion and to T2D [9] and has been described in several models of the disease
156 [10]. Additionally, variants in mitochondrial DNA (mtDNA) in human populations are
157 associated with altered T2D risk [11]. In animal models, alterations in beta cell mtDNA
158 lead to reduced GSIS, hyperglycaemia and beta cell death [12].

159 Under normal physiological conditions, mitochondria undergo fusion and fission cycles
160 which are essential for quality control and adaptation to energetic demands [13]. Thus,
161 highly inter-connected mitochondrial networks allow communication and interchange
162 of contents between mitochondrial compartments, as well as with other organelles

163 such as the endoplasmic reticulum (ER) [14]. These networks exist interchangeably
164 with more fragmented structures, displaying more “classical” mitochondrial
165 morphology [15]. Mitochondrial fission is necessary for “quality control” and the
166 elimination of damaged mitochondria by mitophagy [16].

167 Whilst the mitofusins MFN1 and MFN2, homologues of the *D. melanogaster* fuzzy
168 onions (*fzo*) and mitofusin (*dmfn*) gene products [17], are GTPases that mediate fusion
169 of the outer mitochondrial membrane (OMM), optic atrophy protein 1 (OPA1) controls
170 that of the inner mitochondrial membrane (IMM). Dynamin related protein 1 (DRP1) is
171 responsible for mitochondrial fission [18]. Other regulators include FIS1, mitochondrial
172 fission factor (MFF) and MiD49/51 [19].

173 Changes in mitochondrial fusion and fission dynamics are observed in the pancreatic
174 beta cell in animal models of diabetes [9, 20], and patients with T2D and obesity exhibit
175 smaller and swollen mitochondria in pancreatic tissue samples [1]. Additionally, toxic
176 islet amyloid polypeptide (IAPP) oligomers, usually co-expressed with insulin in beta
177 cells, were present in both ER and mitochondrial membranes of T2D patients and
178 rodents transgenic for human-IAPP (h-IAPP) [21].

179 Here, we explore the potential impact of mitochondrial fragmentation in the control of
180 insulin secretion. We show that this manoeuvre exerts profound effects on insulin
181 release, glucose homeostasis and Ca^{2+} dynamics. Remarkably, the deficiencies in
182 insulin secretion are largely corrected by incretin hormones, suggesting a possible
183 approach to ameliorating the consequences of mitochondrial fragmentation in some
184 forms of diabetes.
185
186

187 **Methods**

188 **Study approval** C57BL/6J mice were housed in individually ventilated cages in a
189 pathogen-free facility at 22ºC with a 10-14 h light-dark cycle and were fed *ad libitum*
190 with a standard mouse chow diet (Research Diets, New Brunswick, NJ, USA). All *in*
191 *vivo* procedures were approved by the UK Home Office, according to the Animals
192 (Scientific Procedures) Act 1986 with local ethical committee approval under personal
193 project license (PPL) number PA03F7F07 to I.L.

194

195 **Generation of beta cell selective *Mfn1/Mfn2* knockout (β*Mfn1/2* dKO), *Clec16a***
196 **null and Pdx1CreER mice** Animals were purchased and genotyped as described in
197 ESM Methods.

198

199 **mRNA extraction and quantitative reverse transcription PCR** For measurements
200 of mRNA levels, pancreatic islets from control and β*Mfn1/2* dKO mice were isolated
201 by collagenase digestion [22]. Total RNA from islets (50-100) was extracted and
202 reverse transcribed as previously described [23] (see ESM Table 2 for primer details).

203

204 **Tissue DNA extraction and measurement of mitochondrial DNA (mtDNA) copy**
205 **number** Total islet DNA was isolated using Puregene Cell and Tissue Kit (Qiagen,
206 Manchester, UK). See ESM Methods for further details.

207

208 **SDS-PAGE and western blotting** Islets were collected and lysed (20 μg) as
209 previously described [23]. See ESM Methods for details.

210

211 **Intraperitoneal (i.p.) or oral gavage of glucose followed by insulin or ketone**
212 **levels measurement and insulin tolerance assessment *in vivo*** IPGTTs, IPIITTs,
213 OGTTs and plasma insulin measurements were performed as previously described
214 [23] in control and β*Mfn1/2* dKO mice. β-ketones were measured in tail vein blood from
215 fed or fasted (16h) mice using an Area 2K device (GlucoMen, Berkshire, UK).
216
217 ***In vitro* insulin secretion** Isolated islets were subjected to glucose-stimulated insulin
218 secretion as described in ESM Methods.
219
220 **cAMP assay** Total cAMP was measured in primary dispersed mouse islet cells as
221 described in ESM Methods.
222
223 **Single-cell fluorescence imaging** Pancreatic islets were isolated from mice,
224 dissociated into single beta cells and plated onto glass coverslips [24]. See ESM
225 Methods for details.
226
227 **Mitochondrial shape analysis** To determine morphological characteristics of
228 mitochondria, confocal stacks were analysed with ImageJ using an in-house macro
229 (available upon request). See ESM Methods for details.
230
231 **Whole-islet fluorescence imaging** Fluorescence imaging of whole islets was
232 performed as described in ESM Methods.
233

234 **TIRF fluorescence imaging** Experiments using the membrane-located zinc sensor
235 ZIMIR [25] or the genetically-encoded and vesicle-located green marker NPY-Venus
236 were performed as presented in ESM Methods.
237
238 **Pancreas immunohistochemistry** Isolated pancreata were fixed and visualised as
239 described in ESM Methods.
240
241 **Metabolomics/lipidomics** Plasma samples from control and dKO mice were
242 analysed as described in ESM Methods.
243
244 **Measurement of oxygen consumption rate** Seahorse XF96 extracellular flux
245 analyzer (Seahorse Bioscience, Agilent, Santa Clara, CA, USA) was used for intact
246 mouse islets respirometry as described in ESM Methods.
247
248 **Electron microscopy (EM) Fixed** islets were processed as described in ESM
249 Methods.
250
251 ***In vivo* Ca^{2+} imaging of AAV8-INS-GCaMP6s infected endogenous pancreatic**
252 **islets** Pancreatic islets of control and β*Mfn1/2*-KO mice were imaged *in vivo* as
253 described in ESM Methods.
254
255 **Connectivity analysis**
256 **Pearson (*r*)-based connectivity and correlation analyses** Correlation analyses
257 were performed as described in ESM Methods.
258

Monte Carlo-based signal binarisation and data shuffling for identification of highly connected cells Data were analysed using approaches as previously described [26, 27]. For further details see ESM Methods.

RNA-Seq data analysis Processing and differential expression analysis of RNA-Seq data was performed as in [28] and ESM Methods.

Statistics Data are expressed as mean ± SEM unless otherwise stated. Significance was tested by Student's two-tailed t-test and Mann–Whitney correction or two-way ANOVA with Sidak's multiple comparison test for comparison of more than two groups, using GraphPad Prism 8 software (San Diego, CA, USA). $p < 0.05$ was considered significant. Experiments were not randomised or blinded.

271 **Results**

272 **Generation of a conditional β*Mfn1/2* dKO mouse line.** Efficient deletion of *Mfn1*
273 and *Mfn2* in the beta cell was achieved in adult mice using the Pdx1-Cre^{ERT2} transgene
274 and tamoxifen injection at 7-8 weeks. Possession of this transgene alone had no effect
275 on glycaemic phenotype or cellular composition of pancreatic islets (Suppl. Fig.**1A-C**).
276 Deletion of mitofusin genes was confirmed by qRT-PCR (Fig.**1A**) and Western
277 (immuno-) blotting (Fig.**1B**) analysis in 14-weeks old male mice. Relative to *β-actin*,
278 expression of the *Mfn1* and *Mfn2* transcripts in isolated islets from dKO mice
279 decreased by ~83 and 86% accordingly vs control islets (Fig.**1A;** $p<0.01$,$p<0.0001$),
280 consistent with selective deletion in the beta cell compartment [29]. No differences
281 were detected in the expression of other mitochondrial fission and fusion mediator
282 genes such as *Opa1*, *Drp1* and *Fis1* (Fig.**1A**). Body weights also differed between
283 groups after 20-21 weeks (Suppl.Fig.**2A;** $p<0.05$).

284

285 **β*Mfn1/2* dKO mice are glucose intolerant with impaired GSIS *in vivo.*** To study
286 the effects of mitofusin gene deletion in beta cells on systemic glucose homeostasis
287 and insulin secretion *in vivo,* i.p. injections (IPGTT) were performed on β*Mfn1/2* dKO
288 and control mice (Fig.**1C**). Glucose challenge revealed impaired glucose tolerance in
289 dKO mice compared to their control littermates with levels of glucose being higher at
290 most time points following glucose injection (Fig.**1C-D**;$p<0.05$,$p<0.001$). Glucose
291 intolerance was even more prominent in 20-weeks old dKO mice (Suppl. Fig.**2B-C**;
292 $p<0.001$, $p<0.0001$). β*Mfn1/2* dKO mice (with a 27 mmol/l glycaemia at 15 min.;
293 Fig.**1E-F**;$p<0.05$; $p<0.01$; $p<0.001$) showed dramatically lower insulin levels upon
294 glucose challenge vs control animals, indicating a severe insulin secretory deficiency
295 (Fig.**1G-H**,$p<0.01$,$p<0.001$,$p<0.0001$). In contrast, following an oral gavage (Fig.**1I-J**),

296 the plasma insulin levels in dKO mice (with a 27 mmol/l glycaemia at 15min.) were
297 indistinguishable from control animals (Fig.**1K-L**;$p<0.05$; 0 vs 15min. in dKO). Insulin
298 tolerance was unaltered insulin tolerance in β*Mfn1/2* dKO mice vs control littermates
299 (Suppl.Fig.**1D-E**). Nevertheless, dKO mice displayed significantly elevated plasma
300 glucose (Suppl.Fig.**1F)** under both fed and fasted conditions. Additionally, an increase
301 in β-ketones (ketone bodies) was observed in fasted dKO vs control mice
302 (Suppl.Fig.**1G**). These changes were inversely related to plasma insulin levels, which
303 were lower in dKO than control mice under both fed and fasted, conditions
304 (Suppl.Fig.**1H**).
305
306 **Deletion of *Mfn1/2* alters mitochondrial morphology in beta cells.** Mitochondrial
307 morphology was assessed using confocal imaging and digital deconvolution.
308 Mitochondria were elongated in dissociated control beta cells (Fig.**2A**) while the
309 mitochondrial network in dKO cells was highly fragmented (Fig.**2A;** and inset). The
310 number of mitochondria per cell was not altered (Fig.**2B**). Mitochondrial elongation and
311 perimeter were significantly decreased in β*Mfn1/2* dKO cells, while circularity on the
312 other hand, was increased indicative of rounder and smaller organelles (Fig.**2B**;
313 $p<0.0001$). Mitochondrial structure was also evaluated in isolated islets by
314 transmission electron microscopy (TEM), confirming the presence of more highly
315 fragmented mitochondria in dKO mouse islets compared to the control group (Fig.**2C**).
316 Cristae structure and organisation were also markedly altered in β*Mfn1/2* dKO islet
317 cells (Fig.**2C**;enlarged panels and schematic representations).
318
319 ***Mitofusin* deletion leads to modest changes in beta cell mass.**
320 Immunohistochemical analysis of pancreata from dKO mice showed a small but

321 significant (~33%) loss of pancreatic beta (insulin-positive) cells vs the control group
322 (Fig.**3A-B;** $p<0.05$). Alpha (glucagon-positive) cell surface was not affected by the loss
323 of mitofusin genes (Fig.**3C**). However, *Mfn1* and *Mfn2* loss was associated with a
324 ~53% reduction in beta cell-alpha cell ratio (Fig.**3D;** $p<0.05$). In line with these findings,
325 the number of TUNEL-positive beta cells were markedly increased in dKO vs control
326 animals (Fig.**3E-F;**$p<0.05$), suggesting that programmed cell death contributes to the
327 observed decrease in beta cell mass.
328
329 **Beta cell identity is modestly altered in β*Mfn1/2* dKO islets.** Whilst *Ins2*, *Ucn3* and
330 *Glut2* (*Slc2a2*) were significantly downregulated, *Trpm5* was upregulated, in dKO
331 islets (Suppl.Fig.**3**). No changes in α- or beta cell disallowed genes [30] were detected.
332 In contrast, genes involved in mitochondrial function such as *Smdt1* and *Vdac3* were
333 upregulated in β*Mfn1/2* dKO islets, consistent with compromised mitochondrial Ca^{2+}
334 uptake, and ATP production, respectively, in dKO beta cells (Suppl.Fig.**3**). Lastly,
335 genes involved in ER stress and mito/autophagy were also affected by inactivation of
336 *Mfn1* and *Mfn2* with *Chop (Ddit3)* and *p62* being upregulated and *Lc3* and *Cathepsin*
337 *L* downregulated.
338
339 **Glucose-induced cytosolic Ca^{2+} and $\Delta\psi_m$ changes are impaired in β*Mfn1/2* dKO**
340 **beta cells *in vivo.*** Mitochondrial membrane polarisation ($\Delta\psi_m$) and Ca^{2+} dynamics
341 were next studied *in vivo*. Animals previously infected with GCaMP6s, and co-stained
342 with tetramethyl rhodamine methyl ester (TMRM) immediately prior to data capture,
343 were imaged for 18-30 min. post i.p. injection of glucose in control (Fig.**4A**;
344 Suppl.Fig.**4A**) and dKO mice (Fig.**4B**; Suppl.Fig.**4B**). Imaging revealed cytosolic Ca^{2+}
345 oscillations ($[Ca^{2+}]_{cyt}$; upward traces) and synchronous mitochondrial membrane

346 depolarisation (downward traces; TMRM positive organelles) in response to elevated
347 glucose in control beta cells. These were largely abolished in dKO islets in response
348 to glucose (Fig.**4B**;Suppl.Fig.**4B**). Measurement of the AUC of fold change traces
349 above baseline depicted significantly impaired GCaMP6s spike signals in response to
350 glucose (Fig.**4C**;$p<0.001$ and $p<0.05$; Suppl.Fig.**4C**) and a tendency towards less
351 TMRM uptake in dKO islets (Fig.**4D**).
352
353 **Mitofusins are essential to maintain normal glucose-stimulated Ca^{2+} dynamics,**
354 **mitochondrial membrane potential and ATP synthesis in beta cells.** Increased
355 cytosolic Ca^{2+} is a major trigger of insulin exocytosis in response to high glucose [4].
356 dKO mouse islets exhibited a significantly lower increase in $[Ca^{2+}]_{cyt}$ compared to
357 control islets (Fig.**5A-C;**$p<0.01$). When the K_{ATP} channel opener diazoxide and a
358 depolarising K^+ concentration (20 mmol/l KCl) were then deployed together to bypass
359 the regulation of these channels by glucose, cytosolic Ca^{2+} increases were not
360 significantly impaired in dKO compared to control animals (Fig.**5B-C**). A substantial
361 reduction in mitochondrial free Ca^{2+} concentration ($[Ca^{2+}]_{mito}$) in response to 17 mmol/l
362 glucose [23, 31] was also observed in dKO islets (Fig.**5D-F;** $p<0.05$). Of note,
363 subsequent hyperpolarisation of the plasma membrane with diazoxide caused the
364 expected lowering of mitochondrial $[Ca^{2+}]_{mito}$ in control islets (reflecting the decrease
365 in $[Ca^{2+}]_{cyt}$;**Fig.5E-F**), but was almost without effect on dKO islets.
366
367 Glucose-induced increases in $\Delta\psi_m$ were also sharply reduced in dKO vs control
368 mouse islets (Fig.**5G-H;** $p<0.01$**).** Addition of 2-[2-[4-
369 (trifluoromethoxy)phenyl]hydrazinylidene]-propanedinitrile (FCCP) resulted in a
370 similar collapse in apparent $\Delta\psi_m$ in islets from both genotypes (Fig.**5G**). To assess

371 whether mitochondrial fragmentation may impact glucose-induced increases in
372 mitochondrial ATP synthesis we performed real-time fluorescence imaging using
373 Perceval (Fig.**5I-J**). While control islets responded with a time-dependent rise in the
374 ATP:ADP ratio in response to a step increase in glucose from 3 mmol/l to 17 mmol/l,
375 β*Mfn1/2* dKO beta cells failed to mount any response (Fig.**5J**;$p< 0.05$).
376
377 **Beta cell-beta cell connectivity is impaired by *Mfn1/2* ablation.** Intercellular
378 connectivity is required in the islet for a full insulin secretory response to glucose [10,
379 26]. To assess this, individual Ca^{2+} traces recorded from Cal-520-loaded beta-cells in
380 mouse islets (Fig.**5A-B**) were subjected to correlation (Pearson *r*) analysis to map cell-
381 cell connectivity (Suppl.Fig.**5A**). Following perfusion at 17 mmol/l glucose, β*Mfn1/2*
382 dKO beta cells tended to display an inferior, though not significantly different,
383 coordinated activity than control cells, as assessed by counting the number of
384 coordinated cell pairs (Suppl.Fig.**5C**; 0.94 vs 0.90 for control vs dKO, respectively). By
385 contrast, beta cells displayed highly coordinated Ca^{2+} responses upon addition of 20
386 mmol/l KCl in dKO islets. Similarly, analysis of correlation strength in the same islets
387 revealed significant differences in response to 17 mmol/l glucose between genotypes.
388 In fact, dKO islets had weaker mean beta-beta cell coordinated activity (Suppl. Fig.**5B,**
389 **D**; $p<0.05$; 0.88 vs 0.77 for control vs dKO, respectively), indicating that mitofusins
390 affect the strength of connection rather than the number of coordinated beta cell pairs.
391 A tending towards lower expression of the gap junction gene *Cx36/Gjd2* has also been
392 observed in dKO islets (Suppl.Fig.**5E**).
393
394 Clear adherence to a power law distribution of connected beta cells [26, 27] was
395 apparent in the control islet group in the elevated glucose condition where 5.70% of

396 the beta cells hosted at least 60% of the connections with the rest of the beta cells
397 ('hubs';Suppl.Fig.**6;** R^2=0.15). No clear adherence to a power-law distribution of
398 connected beta cells was present in the dKO group (R^2=0.002) despite displaying a
399 higher percentage (15.06%) of beta cell-beta cell connections.
400
401 **Unaltered ER Ca^{2+} mobilisation but decreased mitochondrial O_2 consumption**
402 **and mtDNA depletion in β*Mfn1/2* dKO islets.** No differences in cytosolic Ca^{2+}
403 responses between genotypes were observed after agonism at the Gq-coupled
404 metabotropic acetylcholine (Ach) receptor (Fig.**6A-C**). In contrast, measurements of
405 O_2 consumption revealed that both basal and glucose-stimulated mitochondrial
406 respiratory capacities were significantly impaired in dKO islets (Fig.**6D-E**). Moreover,
407 dKO islets displayed a ~75% reduction in mtDNA (Fig.**6F**;p<0.05).
408
409 **Impaired GSIS *in vitro* and beta cell connectivity can be rescued by incretins in**
410 **β*Mfn1/2* dKO mouse islets**. While GSIS was markedly impaired in dKO islets
411 (Fig.**7A**;p<0.05), incretins (GLP-1 or GIP), or the GLP1R agonist exendin-4, at a
412 submaximal concentration of 10 mmol/l glucose, led to a significant potentiation in
413 GSIS in both groups (control: 3G vs ex4; p<0.05 and dKO: 3G vs ex4; p<0.0001, or
414 3G vs GLP-1; p<0.001, or 3G vs GIP; p<0.001). Consequently, insulin secretion in
415 response to 10 mmol/l glucose was no longer different between control and β*Mfn1/2*
416 dKO islets after incretin addition (Fig.**7A-B**). Moreover, under these conditions, forced
417 increases in intracellular cAMP imposed by the addition of FSK or IBMX, which
418 activate adenylate cyclase (AC) and inhibit phosphodiesterase (PDE) respectively,
419 also eliminated differences in GSIS between the genotypes (Fig.**7B**). No differences

420 in insulin secretion were observed between control and dKO islets after depolarisation
421 with KCl.
422
423 We next explored whether the incretin-mediated improvements in insulin secretion in
424 response to incretins were the result of altered $[Ca^{2+}]_{cyt}$ dynamics. Islets from isolated
425 dKO mice displayed a delayed increase in $[Ca^{2+}]_{cyt}$ in response to 10 mmol/l glucose
426 compared to control islets (Fig.**7C-D**; p=0.09; AUC control: 10G vs ex4; p<0.05; dKO:
427 10G vs ex4; p<0.001; ex4 vs KCl; p<0.05). Addition of exendin-4 led to the emergence
428 of oscillatory activity in both groups and under these conditions, differences between
429 genotypes, as seen in Fig.**5B**, were no longer evident (Fig.**7C**). Measured at 10mmol/l
430 glucose, control and dKO islets displayed increases in ER Ca^{2+} in response to
431 exendin-4 (Fig.**7E-F**; AUC;p<0.001) while the response exaggerated in the latter
432 group. Neither group displayed significant changes in ATP:ADP ratio in response to
433 exendin-4 (Fig.**7G-H**;AUC;p<0.01). Analysis of OCR revealed no significant
434 differences between genotypes at 10mmol/l glucose in the presence or absence of
435 exendin-4 or FSK (Fig.**7I**; p<0.05). Finally, exendin-4 sharply increased beta cell-beta
436 cell connectivity in dKO, but not in control islets, as assessed by monitoring Ca^{2+}
437 dynamics and the number of correlated cell pairs (Fig. **8A,C**) or Pearson *r* value (Fig.
438 **8B,D**).
439
440 **Insulin secretion is rescued by incretins through an EPAC-dependent activation.**
441 Neither basal nor incretin-stimulated cAMP levels differed between control and dKO
442 groups (Fig.**9A**). Nonetheless, insulin secretion was amplified in the presence of the
443 protein kinase A (PKA) inhibitor H89 alone or in addition to IBMX and FSK in dKO
444 islets (Fig.**9B**; p<0.05, p<0.01, p<0.001). Insulin secretion was further increased in

445 dKO islets when EPAC was selectively activated, while PKA was inhibited by H89
446 (Fig.**9C**; p<0.05).
447
448 **Defective glucose-stimulated insulin secretion is rescued by GLP-1R agonism**
449 **in *Clec16a* null mice.** To determine whether incretins may reverse defective insulin
450 secretion in an alternative model of mitochondrial dysfunction, we examined mice
451 lacking the mitophagy regulator *Clec16a* selectively in the pancreatic islet
452 (*Clec16a*$^{\Delta panc}$) [32]. Glucose-stimulated insulin secretion was sharply inhibited in null
453 vs Pdx1-Cre control mice, and these differences between genotype were largely
454 corrected in by the addition of exendin-4 (Suppl. Fig.**7A**; p<0.0001). Correspondingly,
455 whereas the difference between *Clec16a*$^{\Delta panc}$ and control mice was significant for
456 IPGTTs there was no such (significant) difference for the OGTTs at 15mins, in line
457 with the findings above for β*Mfn1/2* dKO mice (Suppl. Fig.**7B-C**; p<0.05, p<0.01).
458
459 **Defective secretion of a preserved pool of morphologically-docked granules in**
460 **β*Mfn1/2* dKO mouse beta cells**. To determine whether the markedly weaker
461 stimulation of insulin secretion in dKO islets may reflect failed recruitment of secretory
462 granules into a readily releasable or morphologically-docked pool beneath the plasma
463 membrane, we next deployed total internal reflection fluorescence (TIRF) microscopy
464 in dissociated beta cells. By over-expressing the secretory vesicle marker
465 neuropeptide Y-Venus (NPY-Venus), the number of insulin granules was significantly
466 higher in close proximity with the plasma membrane in dKO cells after treatment with
467 20 mmol/l KCl (Suppl.Fig.**8A-B;**p<0.05**).** However, when we then used the cell
468 surface-targeted Zinc indicator to monitor induced exocytotic release (ZIMIR) [25] in

469 response to depolarisation as a surrogate for insulin secretion, release events were
470 fewer in number and smaller in dKO (Suppl.Fig.**8C-E**).

471 **Altered plasma metabolomic and lipidomic profiles in β*Mfn1/2* dKO mice.** We
472 applied an -omics approach to study metabolite and lipid changes in peripheral plasma
473 samples from control and dKO mice (Suppl.Fig.**9**). Of 29 metabolites, the levels of five
474 metabolic species (shown in red) were significantly altered in β*Mfn1/2* dKO compared
475 to control animals (Suppl.Fig.**9A;** $p<0.05$;$p<0.01$). In the lipidomics analysis, 298 lipid
476 species from 17 different classes were studied. When comparing dKO to control
477 samples, the majority of lipid classes displayed a remarkably homogeneous downward
478 trend of the individual lipid species they comprised (Suppl.Fig.**9B;** $p<0.05$;$p<0.01$).

479 **Changes in *Mfn1* and *Mfn2* expression in mouse strains maintained on regular**
480 **chow or high fat high sugar (HFHS) diet.** To determine whether the expression of
481 *Mfn1* or *Mfn2* might be affected under conditions of hyperglycaemia mimicking T2D in
482 humans, we interrogated data from a previous report [33] in which RNA sequencing
483 was performed on six mouse strains. BALB/cJ mice showed “antiparallel” changes in
484 *Mfn1* and *Mfn2* expression in response to maintenance on high fat high sugar (HFHS)
485 diet for 10 days, and similar changes were obtained in DBA/2J mice at 30 and 90 days
486 (Suppl.Fig.**10A-B**).

487 **Discussion**

488 The key goal of the present study was to determine the impact of disrupting
489 mitochondrial dynamics on glucose- and incretin-stimulated insulin secretion. Deletion
490 of both mitofusin isoforms selectively from the adult beta cell led to fragmentation of
491 the mitochondrial network, impaired glucose signalling and altered beta cell identity.
492 These changes were associated with marked dysglycaemia, which worsened with
493 age. We chose the above strategy over the deletion of either mitofusin gene alone
494 given the similar levels of expression of both in the beta cell [34] and the likelihood of
495 at least partial functional redundancy as reported in [35]. Specifically, this recent report
496 [35], using a complementary strategy (deletion with the constitutive Ins1*Cre* deleter
497 strain), supports this view, demonstrating minor phenotypic effects of deletion in the
498 beta cell of *Mfn1* or *Mfn2* alone.

499

500 The present study shows for the first time that collapse of the mitochondrial network
501 prompted by the loss of *Mfn1* and *Mfn2* has a drastic impact on beta cell function. Our
502 findings are in line with earlier studies which provided evidence for a critical role for
503 preserved mitochondrial dynamics in insulin secretion [36, 37]. In these earlier studies,
504 deletion of *Drp1* from primary mouse beta cells resulted in glucose intolerance,
505 impaired GSIS and abnormal mitochondrial morphology. Conversely, over-expression
506 of DRP1 in clonal INS1 cells decreased GSIS and increased the levels of apoptosis
507 [38], suggesting that a balance between fission and fusion is critical to avoid
508 pathological changes. Finally, mice deficient for *Opa1* in the beta cell develop
509 hyperglycaemia, and show defects in the electron transport chain complex IV, Ca^{2+}
510 dynamics, and insulin secretion [2]. None of the above studies explored the effects on
511 incretin-stimulated secretion.

512 A striking finding in the present report is that, in contrast to results during
513 intraperitoneal glucose injection, insulin secretion and glucose excursion were largely
514 normal in dKO mice during OGTTs, where an incretin effect is preserved [7]. Incretins
515 act, at least in large part, by increasing intracellular cAMP, and adequate cAMP levels
516 are required for the normal stimulation of insulin secretion as glucose concentrations
517 rise [7]. Conversely, incretin action requires adequate glucose levels (and hence
518 intracellular metabolism of the sugar) [7]. Others [39, 40] have previously suggested
519 that cAMP-raising agents may rescue the metabolic signalling defects associated with
520 T2D. However, we are not aware of any previous studies which have *selectively*
521 interfered with mitochondrial function, and then explored the ability of incretins to
522 induce a reversal of the secretory deficiency.
523
524 What mechanisms might explain the ability of incretins to bypass defective insulin
525 secretion after disruption of mitochondrial networks? Explored in dissociated islets,
526 cAMP levels were not different between control and dKO animals in the absence or
527 presence of hormones or GLP1R agonists. cAMP acts at multiple points in the
528 secretory pathway, regulating plasma membrane excitability and Ca^{2+} dynamics
529 (partly via exchange protein activated by cAMP and mainly EPAC2 translocation to
530 granule docking sites on the plasma membrane) [40-42] and also on the exocytotic
531 machinery via N-ethylmaleimide-sensitive attachment receptor (SNARE) proteins [43].
532 Here we show that insulin secretion stimulated by incretins is potentiated in dKO cells
533 through an EPAC-dependent activation, while PKA has an inhibitory effect on
534 secretion. It is still unknown how fragmented mitochondria are associated with the
535 positive regulation of insulin secretion by EPAC and more studies need to be
536 undertaken to explore this phenomenon. Synaptotagmin-7, another critical regulator

537 of Ca^{2+}-mediated exocytosis in beta cells, is known to be phosphorylated and activated
538 by PKA [40], and may thus represent a potential target for incretin action in dKO cells.
539 No difference in mobilization of Ca^{2+} was observed between groups using the IP3R
540 agonist Ach, implying that ER Ca^{2+} stores are not depleted. Nevertheless, by mitofusin
541 deletion, perifusion of exendin-4 revealed that Ca^{2+} accumulation in the ER was higher
542 in dKO cells. This could be associated with a rapid mobilisation and increase in
543 $[Ca^{2+}]_{cyt}$ oscillatory response that lead to an enriched pulsatile insulin secretion and
544 beta cell connectivity [44]. Moreover, since $[Ca^{2+}]_m$ uptake was impaired in dKO cells
545 and maintaining a high $[Ca^{2+}]_{ER}$ is important for beta cell function and survival, the ER
546 could work as a rescue machinery to avoid $[Ca^{2+}]_{cyt}$ overload and toxicity or
547 inflammatory stress [44].
548
549 Of note, impaired glucose-induced ATP synthesis and O_2 consumption seen in
550 fragmented dKO mitochondria were not recovered by incretins (at least under
551 10mmol/l glucose). This suggests that the acute rescue of insulin secretion is, to a
552 substantial extent, independent of (and thus downstream to) changes in mitochondrial
553 oxidative metabolism, in line with reports [45] that O_2 consumption is only weakly
554 affected by incretins in wild-type islets.
555
556 Importantly, we demonstrate that preserved mitochondrial ultra-structure is critical for
557 normal beta cell-beta cell connectivity [27]. The mechanisms underlying these
558 changes are, however, unclear but could be associated with altered *Cx36/Gjd2*
559 expression, phosphorylation or activity, and hence the formation of gap junctions
560 between beta cells [46]. Of note, highly connected “hub” [26] and leader [27] beta cell
561 populations have been proposed to be particularly reliant on mitochondrial function

562 [27]. Nevertheless, we did not observe any loss of hierarchical behaviour or apparent
563 hub cell number in dKO mice.
564
565 Metabolomic analyses revealed that the dKO mouse provides a useful model of
566 defective beta cell function observed, to differing extents, in both type 1 and type 2
567 diabetes [47-49].
568
569 Might changes in *Mfn1* and *Mfn2* expression be involved in diabetes development in
570 rodents or humans? Changes in the expression of both genes were observed in two
571 mouse models of the disease, in line with previous findings in beta cells
572 overexpressing h-IAPP [21]. However, we are not aware of studies reporting changes
573 in the expression of human *MFN1* or *MFN2* in human beta cells in this setting.
574
575 Our findings show that acute treatment with incretins, commonly used as treatments
576 for T2D and obesity [7], largely reverses the deficiencies in insulin secretion and
577 cytosolic Ca^{2+} signalling. We also demonstrate that highly selective impairments of
578 mitochondrial function in beta cells can be rescued or bypassed by incretin treatment,
579 and suggest that this might be an important mechanism of action for this drug class.

580 **Acknowledgements**

581 We thank Stephen M. Rothery from the Facility for Imaging by Light Microscopy (FILM)
582 at Imperial College London for support with confocal and widefield microscopy image
583 recording and analysis. We also thank Aida Di Gregorio from the National Heart and
584 Lung Institute (Imperial College) for genotyping the mice.

585

586 **Data Availability.**

587 Not applicable.

588

589 **Funding**

590 GAR was supported by a Wellcome Trust Senior Investigator Award (098424AIA) and
591 Investigator Award (212625/Z/18/Z), MRC Programme grants (MR/R022259/1,
592 MR/J0003042/1, MR/L020149/1), an Experimental Challenge Grant (DIVA,
593 MR/L02036X/1), an MRC grant (MR/N00275X/1), and a Diabetes UK grant
594 (BDA/11/0004210, BDA/15/0005275, BDA16/0005485). IL was supported by a
595 Diabetes UK project grant (16/0005485). This project has received funding from the
596 Innovative Medicines Initiative 2 Joint Undertaking, under grant agreement no. 115881
597 (RHAPSODY). This Joint Undertaking receives support from the European Union's
598 Horizon 2020 research and innovation programme and EFPIA. This work is supported
599 by the Swiss State Secretariat for Education, Research and Innovation (SERI), under
600 contract no. 16.0097. AT was supported by MRC project grant MR/R010676/1.
601 Intravital imaging was performed using resources and/or funding provided by National
602 Institutes of Health grants R03 DK115990 (to AKL), Human Islet Research Network
603 UC4 DK104162 (to AKL; RRID:SCR_014393). BJ acknowledges support from the
604 Academy of Medical Sciences, Society for Endocrinology, The British Society for

605 Neuroendocrinology, the European Federation for the Study of Diabetes, an EPSRC
606 capital award and the MRC (MR/R010676/1). SAS was supported by the JDRF (CDA-
607 2016-189, SRA-2018-539, COE-2019-861), the NIH (R01 DK108921, U01
608 DK127747), and the US Department of Veterans Affairs (I01 BX004444).
609

610 **Author contributions**

611 EG performed experiments and analysed data. EG supported the completion of
612 confocal and widefield microscopy and analysis. ATC performed the EM sample
613 processing and data analysis. CM, MM and AKL were responsible for the *in vivo*
614 intravital Ca^{2+} imaging in mice. PC contributed to the analysis and manipulation of the
615 *in vivo* intravital Ca^{2+} measurements as well as the preparation and imaging of TIRF
616 samples. TS contributed to the generation of the MATLAB script used for connectivity
617 analysis. FYSW and YA generated and performed Monte Carlo-based signal
618 binarisation. BJ performed the cAMP assays. EA and LLN performed the oral gavage
619 in live animals. YX and GG performed studies with Pdx1CreER mice. NA assisted with
620 Seahorse experiment protocols. CLQ and AW contributed to the metabolomics
621 analysis. CCG, CM and MI were responsible for the RNAseq data analysis. SAS
622 performed studies with Clec16a mice. TAR was involved in the design of the floxed
623 *Mfn* alleles. TAR and IL were responsible for the maintenance of mouse colonies and
624 final approval of the version to be published. GAR designed the study and wrote the
625 manuscript with EG with input and final approval of the version to be published from
626 all authors. GAR is the guarantor of this work and, as such, had full access to all the
627 data in the study and takes responsibility for the integrity of the data and the accuracy
628 of the data analysis.
629

630 **Declaration of interests**

631 Authors' relationships and activities GAR has received grant funding and consultancy
632 fees from Les Laboratoires Servier and Sun Pharmaceuticals. The remaining authors
633 declare that there are no relationships or activities that might bias, or be perceived to
634 bias, their work.

635

636 **Electronic Supplemental Information**

637 Supplemental Figures (1-10)

638 Supplemental Figure legends

639 **Electronic Supplemental Tables**

640 **ESM Table 1.** Sequence of primers used for genotyping *Mfn1* and *Mfn2* flox.

641 **ESM Table 2.** List of primers used for qRT-PCR.

642 **ESM Table 3.** Metabolite differences found in plasma samples of control vs dKO mice
643 according to metabolic class and both fold-change and t-test criteria.

644 **ESM videos 1- 6**

References

1. Masini, M., Et Al., Ultrastructural Alterations Of Pancreatic Beta Cells In Human Diabetes Mellitus. Diabetes/Metabolism Research And Reviews, 2017. 33(6): P. E2894.
2. Zhang, Z., Et Al., The Dynamin-Related Gtpase Opa1 Is Required For Glucose-Stimulated ATP Production In Pancreatic Beta Cells. Mol Biol Cell, 2011. 22(13): P. 2235-45.
3. Anderson, A.J., Et Al., Mitochondria-Hubs For Regulating Cellular Biochemistry: Emerging Concepts And Networks. Open Biology, 2019. 9(8): P. 190126-190126.
4. Rutter, G.A., Et Al., Pancreatic B-Cell Identity, Glucose Sensing And The Control Of Insulin Secretion. Biochem J, 2015. 466(2): P. 203-18.
5. Rorsman, P. And F.M. Ashcroft, Pancreatic B-Cell Electrical Activity And Insulin Secretion: Of Mice And Men. Physiol Rev, 2018. 98(1): P. 117-214.
6. Henquin, J.C., Triggering And Amplifying Pathways Of Regulation Of Insulin Secretion By Glucose. Diabetes, 2000. 49(11): P. 1751-60.
7. Nauck, M.A., Et Al., GLP-1 Receptor Agonists In The Treatment Of Type 2 Diabetes - State-Of-The-Art. Mol Metab, 2020: P. 101102.
8. Jones, B., Et Al., Control Of Insulin Secretion By GLP-1. Peptides, 2018. 100: P. 75-84.
9. Supale, S., Et Al., Mitochondrial Dysfunction In Pancreatic Beta Cells. Trends Endocrinol Metab, 2012. 23(9): P. 477-87.
10. Rutter GA, Et Al., Metabolic And Functional Specialisations Of The Pancreatic Beta Cell: Gene Disallowance, Mitochondrial Metabolism And Intercellular Connectivity. Diabetologia Under Review, 2020.
11. Van Den Ouweland, J.M., Et Al., Functional And Morphological Abnormalities Of Mitochondria Harbouring The Trna(Leu)(UUR) Mutation In Mitochondrial DNA Derived From Patients With Maternally Inherited Diabetes And Deafness (MIDD) And Progressive Kidney Disease. Diabetologia, 1999. 42(4): P. 485-92.
12. Haythorne, E., Et Al., Diabetes Causes Marked Inhibition Of Mitochondrial Metabolism In Pancreatic B-Cells. Nat Commun, 2019. 10(1): P. 2474.
13. Yang, D., Et Al., Mitochondrial Dynamics: A Key Role In Neurodegeneration And A Potential Target For Neurodegenerative Disease. Frontiers In Neuroscience, 2021. 15(359).
14. Rutter, G.A. And R. Rizzuto, Regulation Of Mitochondrial Metabolism By ER Ca2+ Release: An Intimate Connection. Trends In Biochemical Sciences, 2000. 25(5): P. 215-221.
15. Westermann, B., Bioenergetic Role Of Mitochondrial Fusion And Fission. Biochim Biophys Acta, 2012. 1817(10): P. 1833-8.
16. Ma, K., Et Al., Mitophagy, Mitochondrial Homeostasis, And Cell Fate. Front Cell Dev Biol, 2020. 8: P. 467.
17. Filadi, R., Et Al., On The Role Of Mitofusin 2 In Endoplasmic Reticulum-Mitochondria Tethering. Proc Natl Acad Sci U S A, 2017. 114(12): P. E2266-E2267.
18. Rovira-Llopis, S., Et Al., Mitochondrial Dynamics In Type 2 Diabetes: Pathophysiological Implications. Redox Biol, 2017. 11: P. 637-645.
19. Serasinghe, M.N. And J.E. Chipuk, Mitochondrial Fission In Human Diseases. Handb Exp Pharmacol, 2017. 240: P. 159-188.

20. Gao, Y., Et Al., Evaluation Of Mitochondrial Divisions In Mouse With Type-2 Diabetes And Effect Of Glucose-Oxidase On Mouse Islet Cells RIN-M5f. Cell Biol Int, 2014. 38(3): P. 368-73.
21. Safia Costes, T.G., Alexandra E Butler, Sam Sereda, Orian Shirihai And Peter Cawood Butler, Disruption Of The Endoplasmic Reticulum-Mitochondria Interface By Toxic IAPP Oligomers May Compromise Beta-Cell Mitochondrial Network Integrity And Function In Type 2 Diabetes, In The Endocrine Society Annual Meeting, E. Society, Editor. 2015: San Diego.
22. Ravier, M.A. And G.A. Rutter, Isolation And Culture Of Mouse Pancreatic Islets For Ex Vivo Imaging Studies With Trappable Or Recombinant Fluorescent Probes. Methods Mol Biol, 2010. 633: P. 171-84.
23. Georgiadou, E., Et Al., The Pore-Forming Subunit MCU Of The Mitochondrial Ca2+ Uniporter Is Required For Normal Glucose-Stimulated Insulin Secretion In Vitro And In Vivo In Mice. Diabetologia, 2020. 63(7): P. 1368-1381.
24. Tarasov, A.I., Et Al., The Mitochondrial Ca2+ Uniporter MCU Is Essential For Glucose-Induced ATP Increases In Pancreatic B-Cells. PLOS ONE, 2012. 7(7): P. E39722.
25. Li, D., Et Al., Imaging Dynamic Insulin Release Using A Fluorescent Zinc Indicator For Monitoring Induced Exocytotic Release (ZIMIR). Proc Natl Acad Sci U S A, 2011. 108(52): P. 21063-8.
26. Johnston, N.R., Et Al., Beta Cell Hubs Dictate Pancreatic Islet Responses To Glucose. Cell Metab, 2016. 24(3): P. 389-401.
27. Salem, V., Et Al., Leader B-Cells Coordinate Ca2+ Dynamics Across Pancreatic Islets In Vivo. Nature Metabolism, 2019. 1(6): P. 615-629.
28. Cruciani-Guglielmacci, C., Et Al., Molecular Phenotyping Of Multiple Mouse Strains Under Metabolic Challenge Uncovers A Role For Elovl2 In Glucose-Induced Insulin Secretion. Molecular Metabolism, 2017.
29. Elayat, A.A., M.M. El-Naggar, And M. Tahir, An Immunocytochemical And Morphometric Study Of The Rat Pancreatic Islets. J Anat, 1995. 186 (Pt 3)(Pt 3): P. 629-37.
30. Pullen, T.J., M.O. Huising, And G.A. Rutter, Analysis Of Purified Pancreatic Islet Beta And Alpha Cell Transcriptomes Reveals 11β-Hydroxysteroid Dehydrogenase (Hsd11b1) As A Novel Disallowed Gene. Frontiers In Genetics, 2017. 8(41).
31. Mccormack, J.G., A.P. Halestrap, And R.M. Denton, Role Of Calcium Ions In Regulation Of Mammalian Intramitochondrial Metabolism. Physiol Rev, 1990. 70(2): P. 391-425.
32. Soleimanpour, S.A., Et Al., The Diabetes Susceptibility Gene Clec16a Regulates Mitophagy. Cell, 2014. 157(7): P. 1577-1590.
33. Cruciani-Guglielmacci, C., Et Al., Molecular Phenotyping Of Multiple Mouse Strains Under Metabolic Challenge Uncovers A Role For Elovl2 In Glucose-Induced Insulin Secretion. Molecular Metabolism, 2017. 6(4): P. 340-351.
34. Benner, C., Et Al., The Transcriptional Landscape Of Mouse Beta Cells Compared To Human Beta Cells Reveals Notable Species Differences In Long Non-Coding RNA And Protein-Coding Gene Expression. BMC Genomics, 2014. 15(1): P. 620.
35. Sidarala, V., Et Al., Mitofusins 1 And 2 Collaborate To Fuel Pancreatic Beta Cell Insulin Release Via Regulation Of Both Mitochondrial Structure And DNA Content. Biorxiv, 2021: P. 2021.01.10.426151.

36. Reinhardt, F., Et Al., Drp1 Guarding Of The Mitochondrial Network Is Important For Glucose-Stimulated Insulin Secretion In Pancreatic Beta Cells. Biochem Biophys Res Commun, 2016. 474(4): P. 646-651.
37. Hennings, T.G., Et Al., In Vivo Deletion Of Beta-Cell Drp1 Impairs Insulin Secretion Without Affecting Islet Oxygen Consumption. Endocrinology, 2018. 159(9): P. 3245-3256.
38. Stiles, L. And O.S. Shirihai, Mitochondrial Dynamics And Morphology In Beta-Cells. Best Pract Res Clin Endocrinol Metab, 2012. 26(6): P. 725-38.
39. Holz, G.G. And J.F. Habener, Signal Transduction Crosstalk In The Endocrine System: Pancreatic Beta-Cells And The Glucose Competence Concept. Trends Biochem Sci, 1992. 17(10): P. 388-93.
40. Leech, C.A., O.G. Chepurny, And G.G. Holz, Epac2-Dependent Rap1 Activation And The Control Of Islet Insulin Secretion By Glucagon-Like Peptide-1. Vitam Horm, 2010. 84: P. 279-302.
41. Tsuboi, T. And G.A. Rutter, Multiple Forms Of "Kiss-And-Run" Exocytosis Revealed By Evanescent Wave Microscopy. Curr Biol, 2003. 13(7): P. 563-7.
42. Alenkvist, I., Et Al., Recruitment Of Epac2A To Insulin Granule Docking Sites Regulates Priming For Exocytosis. Diabetes, 2017. 66(10): P. 2610-2622.
43. Takahashi, N., Et Al., Post-Priming Actions Of ATP On Ca2+-Dependent Exocytosis In Pancreatic Beta Cells. Proc Natl Acad Sci U S A, 1999. 96(2): P. 760-5.
44. Idevall-Hagren, O. And A. Tengholm, Metabolic Regulation Of Calcium Signaling In Beta Cells. Seminars In Cell & Developmental Biology, 2020. 103: P. 20-30.
45. Peyot, M.-L., Et Al., Glucagon-Like Peptide-1 Induced Signaling And Insulin Secretion Do Not Drive Fuel And Energy Metabolism In Primary Rodent Pancreatic Beta-Cells. Plos One, 2009. 4(7): P. E6221-E6221.
46. Rutter, G.A., Et Al., Metabolic And Functional Specialisations Of The Pancreatic Beta Cell: Gene Disallowance, Mitochondrial Metabolism And Intercellular Connectivity. Diabetologia, 2020. 63(10): P. 1990-1998.
47. Andersén, E., G. Karlaganis, And J. Sjövall, Altered Bile Acid Profiles In Duodenal Bile And Urine In Diabetic Subjects. Eur J Clin Invest, 1988. 18(2): P. 166-72.
48. Staels, B. And V.A. Fonseca, Bile Acids And Metabolic Regulation. Mechanisms And Clinical Responses To Bile Acid Sequestration, 2009. 32(Suppl 2): P. S237-S245.
49. Uchida, K., S. Makino, And T. Akiyoshi, Altered Bile Acid Metabolism In Nonobese, Spontaneously Diabetic (NOD) Mice. Diabetes, 1985. 34(1): P. 79-83.

783 **Figure legends**
784
785 **Fig.1 Generation of a conditional β*Mfn1/2* dKO mouse line which displays a**
786 **highly impaired glucose tolerance *in vivo***. (A) qRT-PCR quantification of *Mfn1,*
787 *Mfn2, Drp1, Opa1* and *Fis1* expression in control and dKO islets relative to *β-actin*
788 (*n*=3-5 mice per genotype in two independent experiments).(B) Western blot analysis
789 demonstrating efficient MFN1 (84 kDa) and MFN2 (86 kDa) deletion relative to
790 GAPDH (36 kDa) in isolated islets (*n*=3-4 mice per genotype in three independent
791 experiments).(C) Glucose tolerance was measured in dKO mice and littermate
792 controls by IPGTT (1 g/kg body weight).(D) Corresponding AUC from (C) (*n*=8 mice
793 per genotype,in 2 independent experiments). (E) Glucose tolerance measured by
794 IPGTT (using 3 g/kg body weight) and (F) the corresponding AUC were assessed in
795 β*Mfn1/2* dKO and control mice (*n*=8 mice per genotype in two independent
796 experiments). (G) Plasma insulin levels during IPGTT in dKO and control mice (*n*=11-
797 12 mice per genotype in three independent experiments) and (H) the corresponding
798 AUC. (I) Glucose tolerance post-oral gavage (3 g/kg body weight) was measured in
799 *n*=8 animals per genotype in two independent experiements.The corresponding AUC
800 is shown in (J). (K) Plasma insulin levels during OGTT in dKO and control mice (*n*=8
801 mice per genotype in two independent experiments) and (L) the corresponding AUC.
802 (Blue, *control* mice; red, *dKO* mice. Data are presented as mean±SEM. *p<0.05;
803 **p<0.01; ***p<0.001; ****p<0.0001 as indicated, or *control* vs *dKO* mice at the time
804 points as indicated in (**K**), analysed by unpaired two-tailed Student's t-test and Mann–
805 Whitney correction or two-way ANOVA test and Sidak's multiple comparisons test. All
806 experiments were performed in 14-week-old male mice.
807
808 **Fig.2 Mitochondrial ultrastructure is altered following *Mfn1/2* deletion.** (A)
809 Confocal images of the mitochondrial network of dissociated beta cells stained with
810 Mitotracker green; scale bar: 5 μm. Lower right panels: magnification of selected
811 areas. (B) Mitochondrial morphology analysis on deconvolved confocal images of
812 dissociated beta cells. A macro was developed to quantify the number of mitochondria
813 per cell and measure the elongation, perimeter and circularity (0: elongated; 1: circular
814 mitochondria) of the organelles in control and dKO animals (*n*=40-54 cells; *n*=3 mice
815 per genotype). (C) Electron micrographs of mitochondria indicated with black arrows
816 in islets isolated from control and dKO mice; scale bars: 1μm. Right panel:

817 magnification of selected areas showing the cristae structure (black arrow heads);
818 scale bar: 0.5 μm. Schematic representation of enlarged mitochondria. Data are
819 presented as mean±SEM. ****p<0.0001 as indicated, analysed by unpaired two-tailed
820 Student's t-test and Mann–Whitney correction. Experiments were performed in 14-
821 week-old male mice.
822
823 **Fig.3 Absence of *Mfn1/2* in beta cells leads to decreased beta cell mass and**
824 **increased beta cell apoptosis.**(A) Representative pancreatic sections
825 immunostained with glucagon (red) and insulin (green); scale bars: 50μm.(B) The beta
826 cell and alpha cell surface (C) measured within the whole pancreatic area in control
827 and dKO mice were determined, as well as the beta/alpha cell ratio in (D), (*n*=79-86
828 islets, 4 mice per genotype; experiment performed in triplicate).(E) Representative
829 confocal images of islets with TUNEL positive (green) apoptotic beta cells (ROI) and
830 insulin (red). Magnification of selected area displaying each fluorescent channel; scale
831 bar: 5μm. DNase I treated sections were used as a positive control in the TUNEL
832 assay. Scale bars: 20μm.(F) Quantification of the percentage of islets containing
833 TUNEL positive cells (*n*=114-133 islets, 4 mice per genotype; experiment performed
834 in triplicate). Data are presented as mean±SEM. *p<0.05, assessed by unpaired two-
835 tailed Student's t-test and Mann–Whitney correction. Experiments were performed in
836 14-week-old male mice.
837
838 **Fig.4 Deletion of Mfn1/2 impairs beta cell function *in vivo*. Representative *in***
839 ***vivo* images of GCaMP6s labelled islets and TMRM stained mitochondria**
840 **surrounded by their vasculature in control and dKO mice**. (A) Representative
841 traces depicting fluorescence intensity of cytosolic Ca^{2+} (GCaMP6s) and mitochondrial
842 TMRM signals in control (ESM Video 1) and (B) dKO animals (ESM Video 2) before
843 and after glucose injection as indicated; scale bars: 45 μm; (*n*=2 animals per
844 genotype). (C) AUC of fold change measurements above baseline for each GCaMP6s
845 and (D) TMRM traces measured (*n*=4-15 total responding cells). Under these
846 conditions, glucose concentrations in control mice were 17.1±2.5 mmol/l and 32.1±3.9
847 mmol/l in dKO animals after glucose injection. Analysis was performed on the most
848 responsive beta cells where oscillations could be detected in both groups.Green,
849 GCaMP6s; red, TMRM signals. Data are presented as mean±SEM. ***p<0.001,

850 assessed by unpaired two-tailed Student's t-test and Mann–Whitney correction.
851 Experiments were performed in 20-week-old male mice.
852
853 **Fig.5 *Mfn1/2* deletion from pancreatic beta cells impairs cytosolic and**
854 **mitochondrial Ca^{2+} uptake and changes mitochondrial potential and ATP**
855 **synthesis *in vitro*.** (A) Each snapshot of isolated control (i–iv) and dKO-derived (v–
856 viii) islets was taken during the time points indicated by the respective arrows in (B).
857 Scale bar: 50 μm. See also ESM Video 3. (B) $[Ca^{2+}]_{cyt}$ traces in response to 3G, 3
858 mmol/l glucose, 17 mmol/l glucose (17G; with or without diazoxide [diaz]) or 20 mmol/l
859 KCl with diaz were assessed following Cal-520 uptake in whole islets. Traces
860 represent mean normalised fluorescence intensity over time (F/F_{min}).(C) The
861 corresponding AUC is also presented (*n*=17-26 islets, 4 mice per genotype); 17G AUC
862 measured between 245 s and 1045 s, 17G+diaz AUC measured between 1200 s and
863 1320 s, and KCl+diaz AUC measured between 1424 s and 1500 s. For each genotype
864 different baselines (ctrl diaz/KCl: 0.95, dKO diaz/KCl: 0.8 were taken into consideration
865 to measure AUCs.(D) Each snapshot of isolated control (i–iv) and dKO-derived (v–viii)
866 islets was taken during the time points indicated by the respective arrows in (E). Scale
867 bar: 50 μm. See also ESM Video 4. (E) $[Ca^{2+}]_{mito}$ changes in response to 17G (with or
868 without diazoxide [diaz]) and 20 mmol/l KCl were assessed in islets following R-GECO
869 infection. Traces represent mean normalised fluorescence intensity over time
870 (F/F_{min}).(F) The corresponding AUC is also shown (*n*=20-23 islets, 3 mice *per*
871 genotype; 17G AUC measured between 270 s and 1100 s, 17G+diaz AUC measured
872 between 1101 s and 1365 s and KCl AUC measured between 1366 s and1500 s).(G)
873 Dissociated beta cells were loaded with TMRE to measure changes in $\Delta\psi_m$, and
874 perifused with 3 mmol/l glucose (3G), 17G or FCCP as indicated. Traces represent
875 normalised fluorescence intensity over time (F/Fmin).(H) AUC was measured between
876 700–730 s (under 17G exposure) from the data shown in (G) (*n*=146-254 cells,3-6
877 mice per genotype).(I) Changes in the cytoplasmic ATP:ADP ratio ([ATP:ADP]) in
878 response to 17 mmol/l glucose (17G) was examined in whole islets using the ATP
879 sensor Perceval.(J) AUC values corresponding to (I) were measured between 418–
880 1400 s (under 17G exposure) (data points from *n*=22-23 islets, 3-6 mice per genotype).
881 Data are presented as mean±SEM. *p<0.05, **p<0.01, assessed by unpaired two-
882 tailed Student's t-test and Mann–Whitney correction or two-way ANOVA test and

883 Sidak's multiple comparisons test. Experiments were performed in 14-week-old male
884 mice.
885
886 **Fig.6 O_2 consumption and mtDNA are deleteriously affected when *Mfn1/2* are**
887 **abolished in beta cells, while $[Ca^{2+}]_{ER}$ mobilisation remains unchanged.** (A) Each
888 snapshot of isolated control (i–v) and dKO-derived (vi–x) islets was taken during the
889 time points indicated by the respective arrows in (B). Scale bar: 50 μm. See also ESM
890 Video 5. (B) Changes in $[Ca^{2+}]_{ER}$ were measured in whole islets incubated with Cal-
891 520 and perifused with 17 mmol/l glucose (17G; with or without diazoxide [diaz]), 17G
892 with 0.1 mmol/l acetylcholine (Ach) and diaz, or 20 mmol/l KCl with diaz (C) AUC
893 values corresponding to (B) were measured (17G AUC measured between 260 s and
894 740 s, 17G+diaz AUC measured between 846 s and 1020 s, 17G+diaz+Ach AUC
895 measured between 1021 s and 1300 s and KCl AUC measured between 1301 s and
896 1500 s) (n=29-31 islets, 3 mice per genotype). (D) Representative oxygen
897 consumption rate (OCR) traces of islets (~10 per well) were acutely exposed to 20
898 mmol/l glucose (final concentration), Oligomycin A (Oligo), FCCP, and Rotenone with
899 Antimycin A (AA) (performed in triplicate, in two independent experiments).(E)
900 Average values for each condition corresponding to (D).(F) The relative mitochondrial
901 DNA copy number was measured by determining the ratio of the mtDNA-encoded
902 gene *mt-Nd1* to the nuclear gene *Ndufv1* (*n*=3 mice per genotype).Data are presented
903 as mean±SEM. *p<0.05, assessed by unpaired two-tailed Student's t-test and Mann–
904 Whitney correction or two-way ANOVA test and Sidak's multiple comparisons test.
905 Experiments were performed in 14-week-old male mice.
906
907 **Fig.7 Impaired insulin secretion can be rescued by GLP-1R agonists *in vitro* by**
908 **increasing cytosolic Ca^{2+} oscillation frequency.** (A) Insulin secretion measured
909 during serial incubations in batches in 3 mmol/l glucose (3G), 10 mmol/l glucose (10G),
910 or 100 nmol/l exendin-4 (ex4), GLP-1 or GIP in presence of 10G or 17 mmol/l glucose
911 (17G) (*n*=4-7 mice per genotype in two independent experiments).(B) Insulin secretion
912 measured during serial incubations in batches in 10 mmol/l glucose (10G),
913 supplemented with 100 nmol/l exendin-4 (ex4), 10 μmol/l FSK or 100 μmol/l IBMX and
914 20 mmol/l KCl (*n*=3 mice per genotype, in two independent experiments). (C) $[Ca^{2+}]_{cyt}$
915 changes in response to 3G, 3 mmol/l glucose, 10 mmol/l glucose (10G; with or without
916 exendin-4 [ex4]) or 20 mmol/l KCl were assessed following Cal-520 uptake in whole

917 islets. Traces represent mean normalised fluorescence intensity over time (F/F_{min}).
918 See also ESM video 6. Dashed ROIs represent fluorescent segments of extended time
919 scales. Both control and dKO traces reveal faster oscillatory frequencies in response
920 to exendin-4. (D) The corresponding AUC is also presented (*n*=19-20 islets, 3 mice
921 per genotype; 10G AUC measured between 200 s and 660 s, 10G+ex4 AUC
922 measured between 800 s and 950 s), and KCl AUC measured between 1200 s and
923 1500 s).(E) Dissociated beta cells were loaded with D4ER to measure changes in
924 $[Ca^{2+}]_{ER}$, and perifused with 10 mmol/l glucose (10G), 10G+ex4 or thapsigargin
925 (10G+thapsi) as indicated. Traces represent corrected ratio values post-linear fitting
926 over time. (F) AUC was measured between 350–900 s (under 10G+ex4) and 900-
927 1300 s (10G+thapsi) from the data shown in (E) (*n*=44-46 cells,4-5 mice per
928 genotype). (G) Changes in cytoplasmic ATP:ADP ratio ([ATP:ADP]) in response to
929 10G or 10G with 100nmol/l ex4 was examined in whole islets.(H) AUC values
930 corresponding to (G) were measured between 185-720s (under 10G exposure) or 721-
931 1200s (under 10G with ex4) (data points from *n*=3 mice per genotype). (I) Average
932 OCR values of islets (~10 per well) that were exposed to 3mmol/l or 10mmol/l glucose
933 (final concentration), 10mmol/l glucose supplemented with ex4, FSK, Oligomycin A
934 (Oligo), FCCP, and Rotenone with Antimycin A (AA) (*n*=3 mice per genotype;
935 experiment performed in duplicate). Data are presented as mean±SEM.
936 *p<0.05;**p<0.01, ****p<0.0001 assessed by two-way ANOVA test and Sidak's
937 multiple comparisons test. Experiments were performed in 14-week-old male mice.
938
939 **Fig.8 The GLP1-R agonist, exendin-4, improves intercellular connectivity in**
940 **βMfn1/2 dKO β-cells.** (A) Representative cartesian maps of control and dKO islets
941 with colour coded lines connecting cells according to the strength of Pearson analysis
942 (colour coded *r* values from 0 to 1, blue to red respectively) under 10mmol/L (10G),
943 10mmol/L with 100nmol/l exendin-4 (10G+ex4) glucose or 20mmol/L KCl; scale bars:
944 40 μm.(B) Representative heatmaps depicting connectivity strength (*r*) of all cell pairs
945 according to the colour coded *r* values from 0 to 1, blue to yellow respectively.(C)
946 Percentage of connected cell pairs at 10G, 10G+ex4 or KCl (*n*=19-20 islets, 3 mice
947 per genotype).(D) *r* values between β-cells in response to glucose, exendin-4 or KCl
948 (*n*=3 mice per genotype).Data are presented as mean±SEM. *p<0.05,**p<0.01,

949 ***p<0.001 assessed by two-way ANOVA test and Sidak's multiple comparisons test.
950 Experiments were performed in 14-week-old male mice.
951
952 **Fig.9 Insulin secretion is rescued through an EPAC-dependent activation in dKO**
953 **islets.** (A) Concentration of cAMP (normalised to FSK) in response to 1,10,100 nmol/l
954 GLP-1, ex4 and GIP stimulation in dissociated islets (*n*=6-7 animals, in 2 independent
955 experiments). (B) Insulin secretion measured during serial incubations in batches in 3
956 mmol/l glucose (3G), 10 mmol/l glucose (10G), or 10 mmol/l glucose supplemented
957 with 10μmol/l H89, 10 μmol/l FSK with 100 μmol/l IBMX or H89 (*n*=3 mice per
958 genotype, in two independent experiments). (C) Insulin secretion measured during
959 serial incubations in batches in 10 mmol/l glucose (10G), or 10 mmol/l glucose
960 supplemented with 6μmol/l EPAC-activator, or EPAC-activator with 10μmol/l H89 (*n*=3
961 mice per genotype, in two independent experiments). Data are presented as
962 mean±SEM. *p<0.05,**p<0.01, ***p<0.001 assessed by two-way ANOVA test and
963 Sidak's multiple comparisons test. Experiments were performed in 14-week-old male
964 mice.

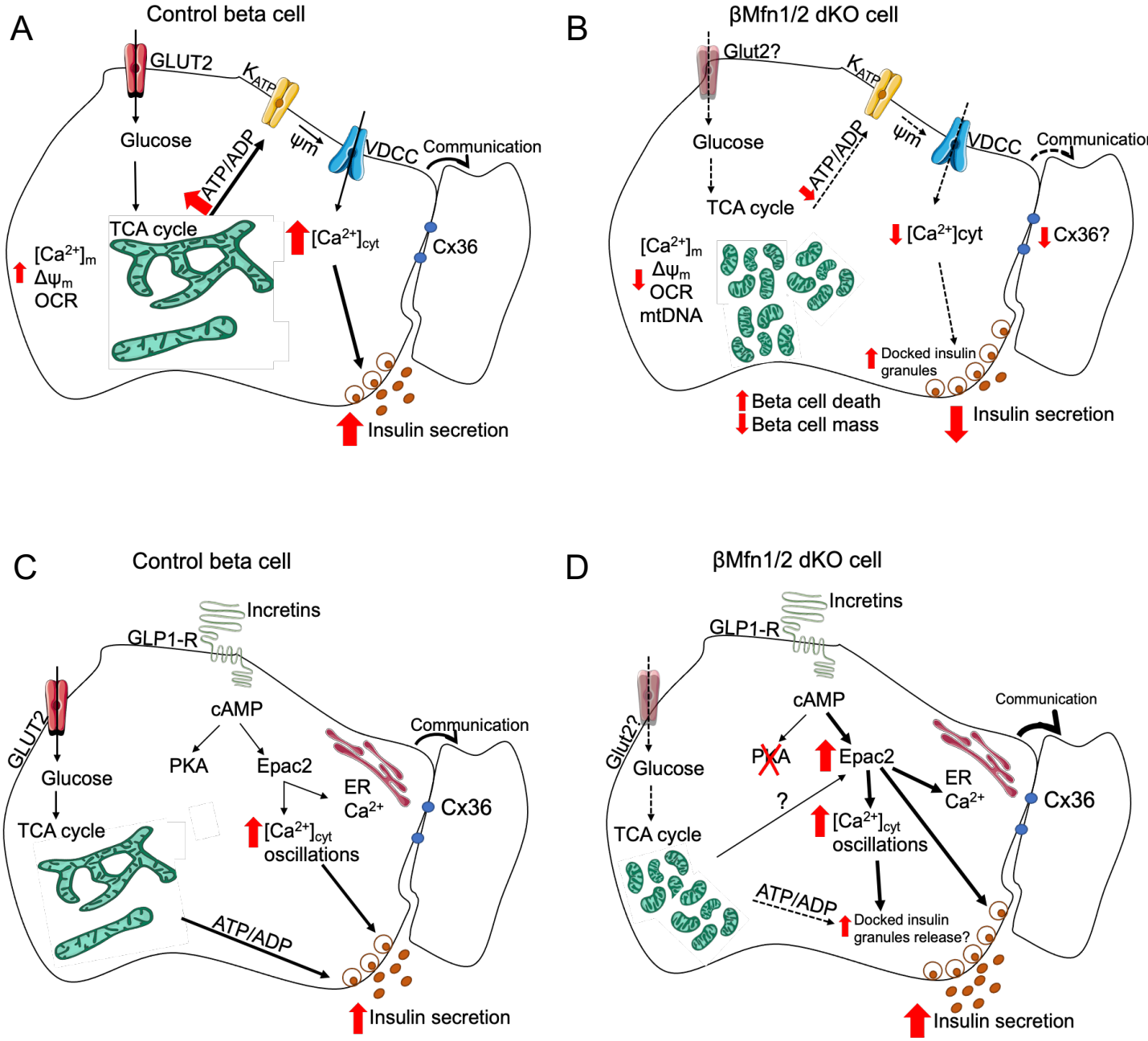

Graphical abstract

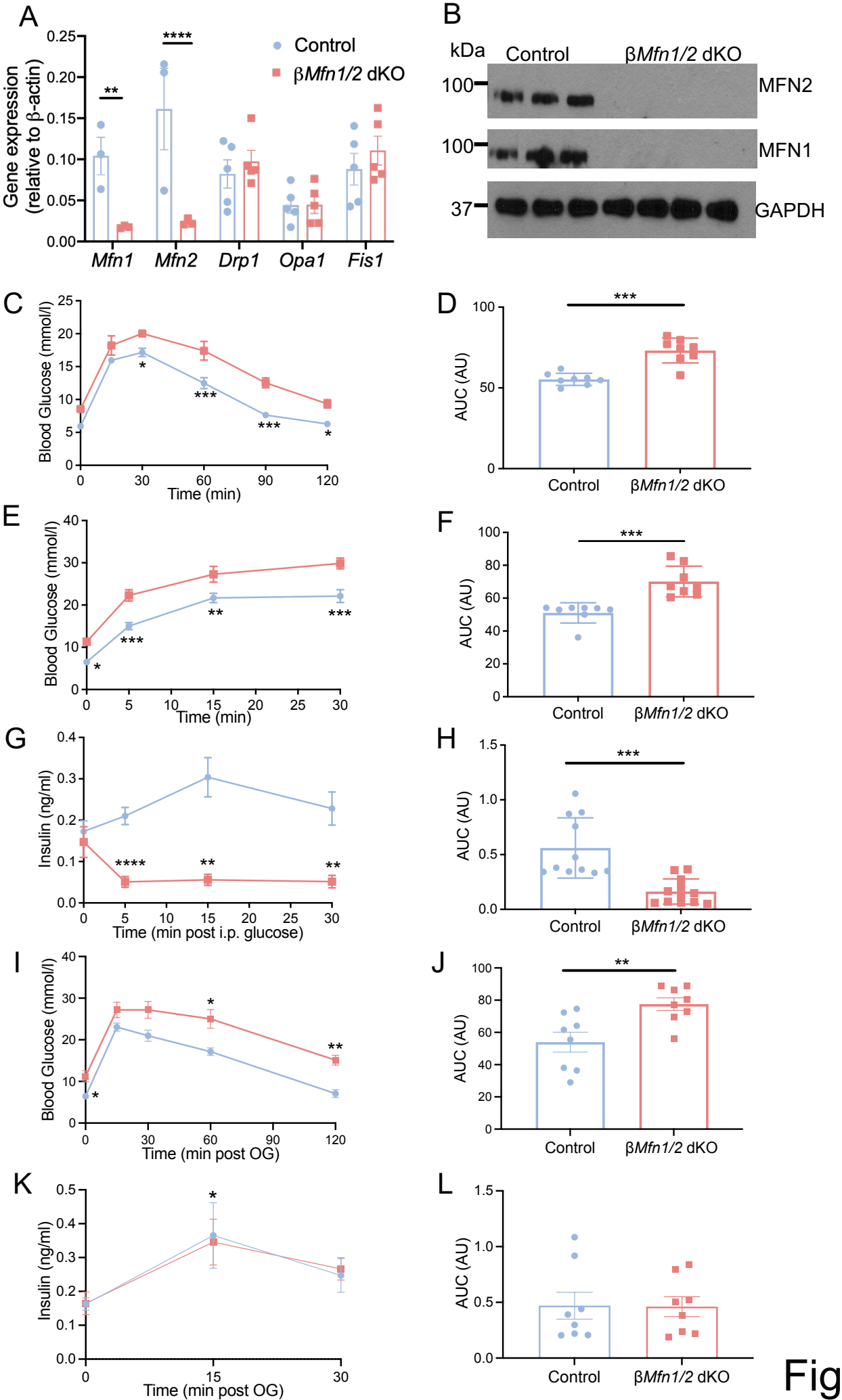
A
Gene expression (relative to β-actin)
Control
βMfn1/2 dKO
Mfn1
Mfn2
Drp1
Opa1
Fis1
B
kDa
Control
βMfn1/2 dKO
100
MFN2
100
MFN1
37
GAPDH
C
Blood Glucose (mmol/l)
Time (min)
D
AUC (AU)
Control
βMfn1/2 dKO
E
Blood Glucose (mmol/l)
Time (min)
F
AUC (AU)
Control
βMfn1/2 dKO
G
Insulin (ng/ml)
Time (min post i.p. glucose)
H
AUC (AU)
Control
βMfn1/2 dKO
I
Blood Glucose (mmol/l)
Time (min post OG)
J
AUC (AU)
Control
βMfn1/2 dKO
K
Insulin (ng/ml)
Time (min post OG)
L
AUC (AU)
Control
βMfn1/2 dKO

Fig.1

A

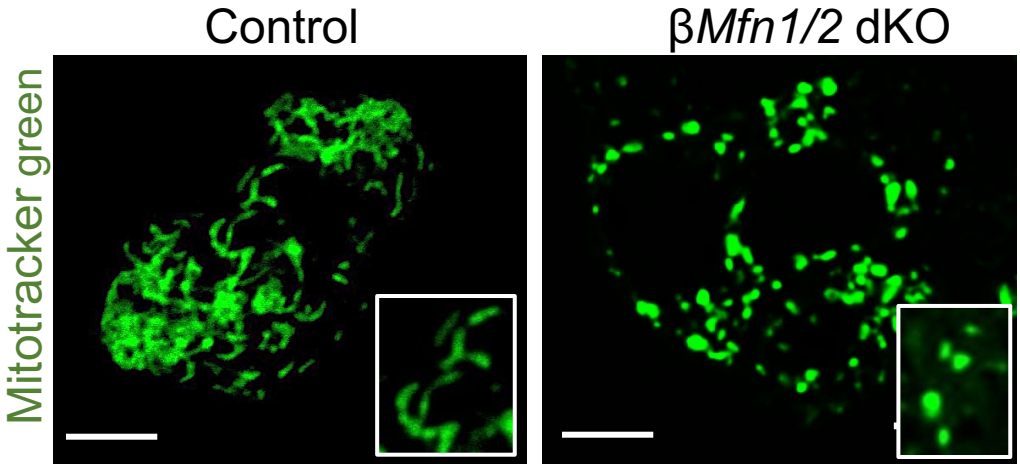
Control
βMfn1/2 dKO
Mitotracker green

B

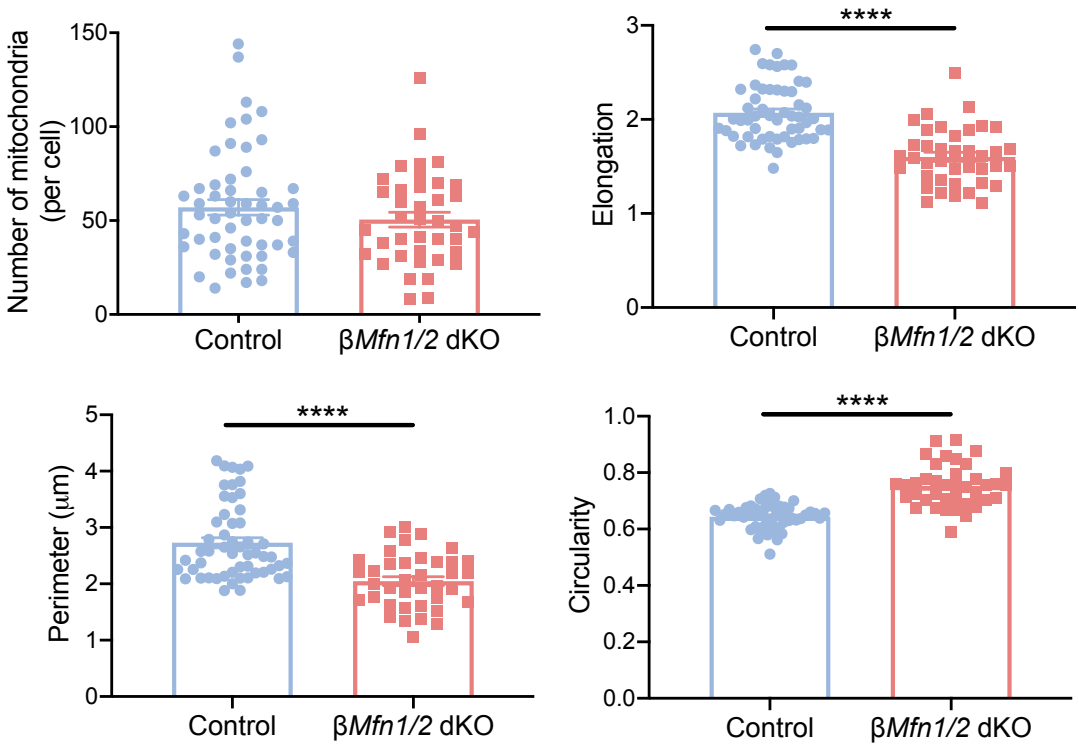
Number of mitochondria (per cell)
150
100
50
0
Control
βMfn1/2 dKO
Elongation
****
3
2
1
0
Control
βMfn1/2 dKO
Perimeter (μm)
****
5
4
3
2
1
0
Control
βMfn1/2 dKO
Circularity
****
1.0
0.8
0.6
0.4
0.2
0.0
Control
βMfn1/2 dKO

C

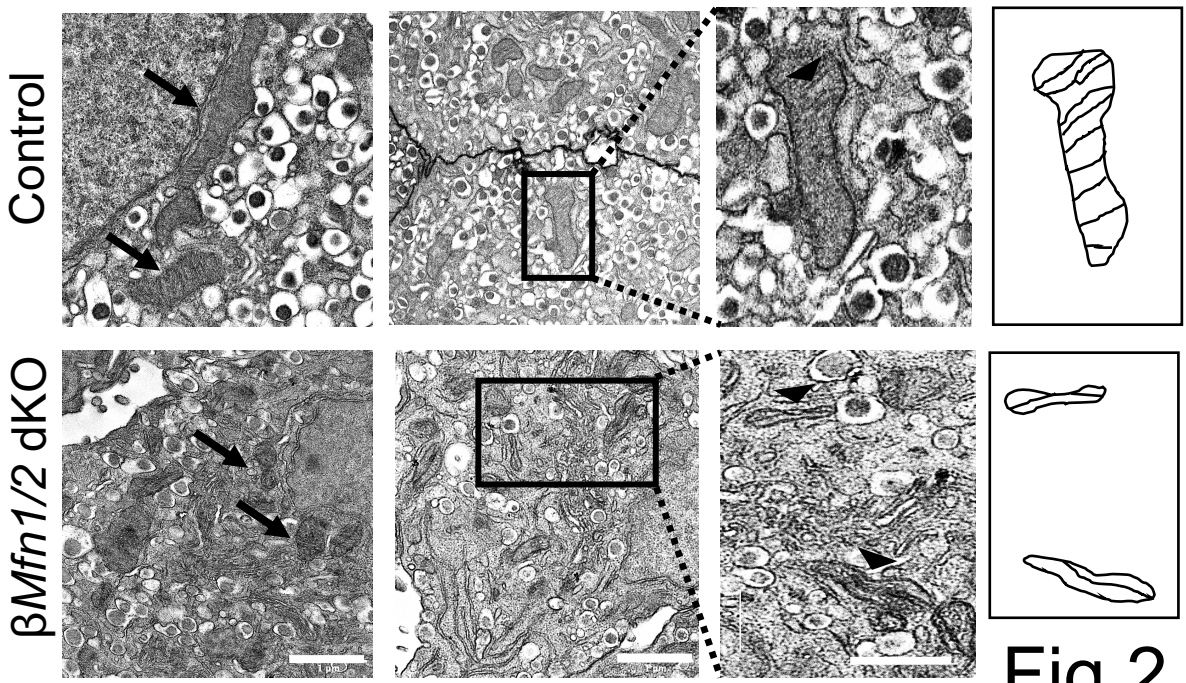
Control
βMfn1/2 dKO

Fig.2

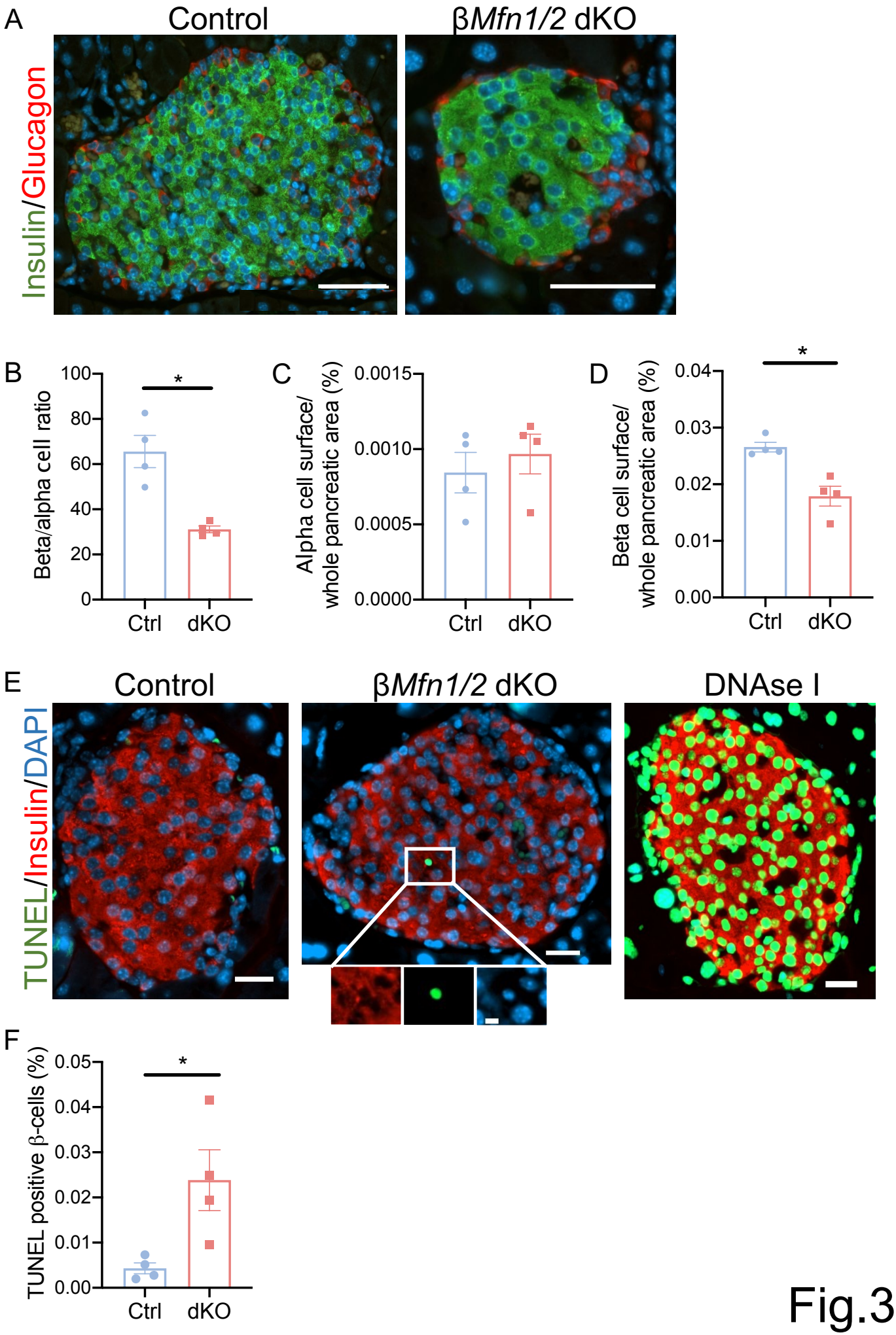
A
Control
βMfn1/2 dKO
Insulin/Glucagon
B
Beta/alpha cell ratio
100
80
60
40
20
0
*
Ctrl
dKO
C
Alpha cell surface/
whole pancreatic area (%)
0.0015
0.0010
0.0005
0.0000
Ctrl
dKO
D
Beta cell surface/
whole pancreatic area (%)
0.04
0.03
0.02
0.01
0.00
*
Ctrl
dKO
E
Control
βMfn1/2 dKO
DNAse I
TUNEL/Insulin/DAPI
F
TUNEL positive β-cells (%)
0.05
0.04
0.03
0.02
0.01
0.00
*
Ctrl
dKO

Fig.3

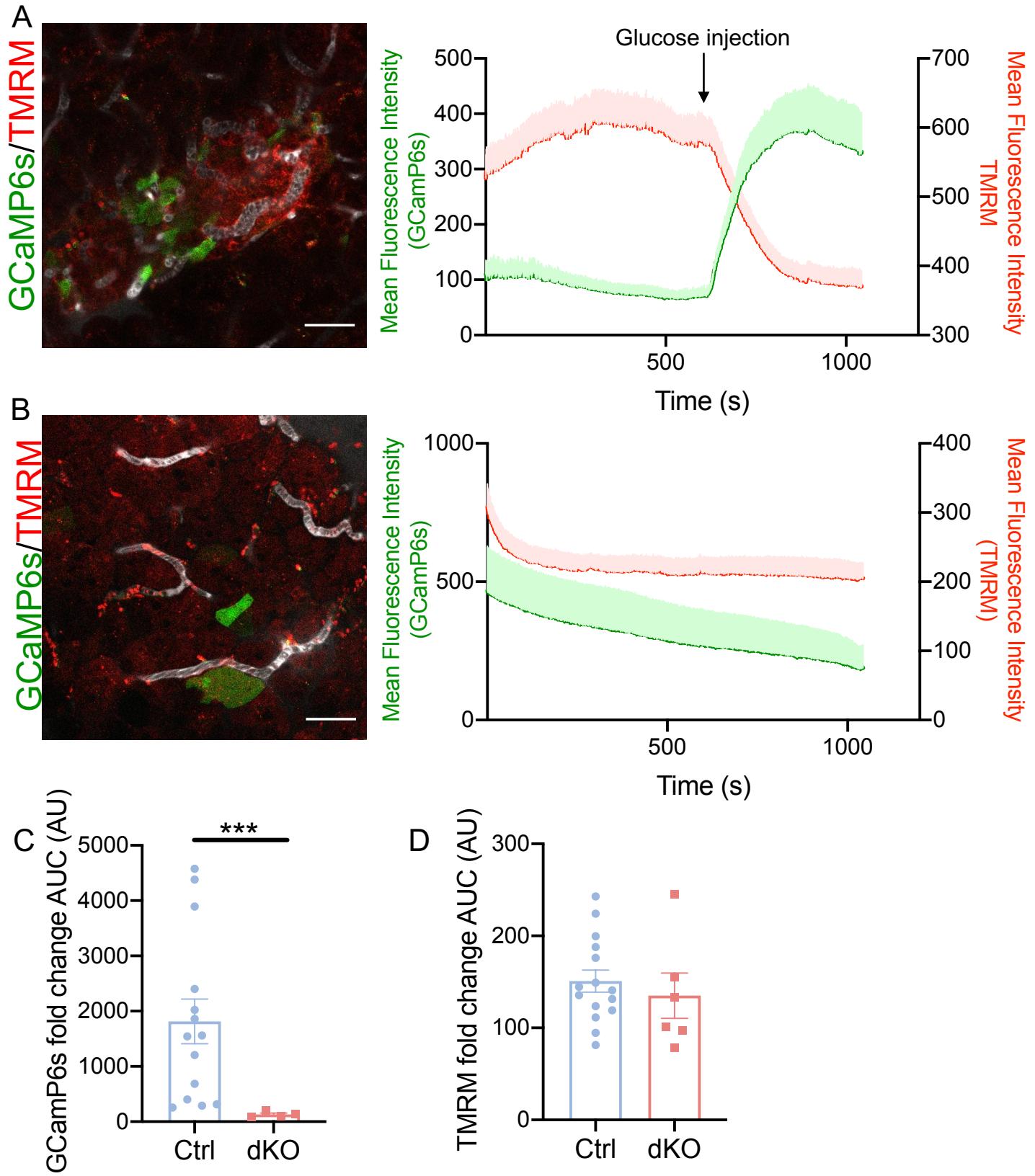
A
GCaMP6s/TMRM
Glucose injection
Mean Fluorescence Intensity (GCamP6s)
Mean Fluorescence Intensity TMRM
Time (s)
B
GCaMP6s/TMRM
Mean Fluorescence Intensity (GCamP6s)
Mean Fluorescence Intensity (TMRM)
Time (s)
C
GCamP6s fold change AUC (AU)
***
Ctrl
dKO
D
TMRM fold change AUC (AU)
Ctrl
dKO

Fig.4

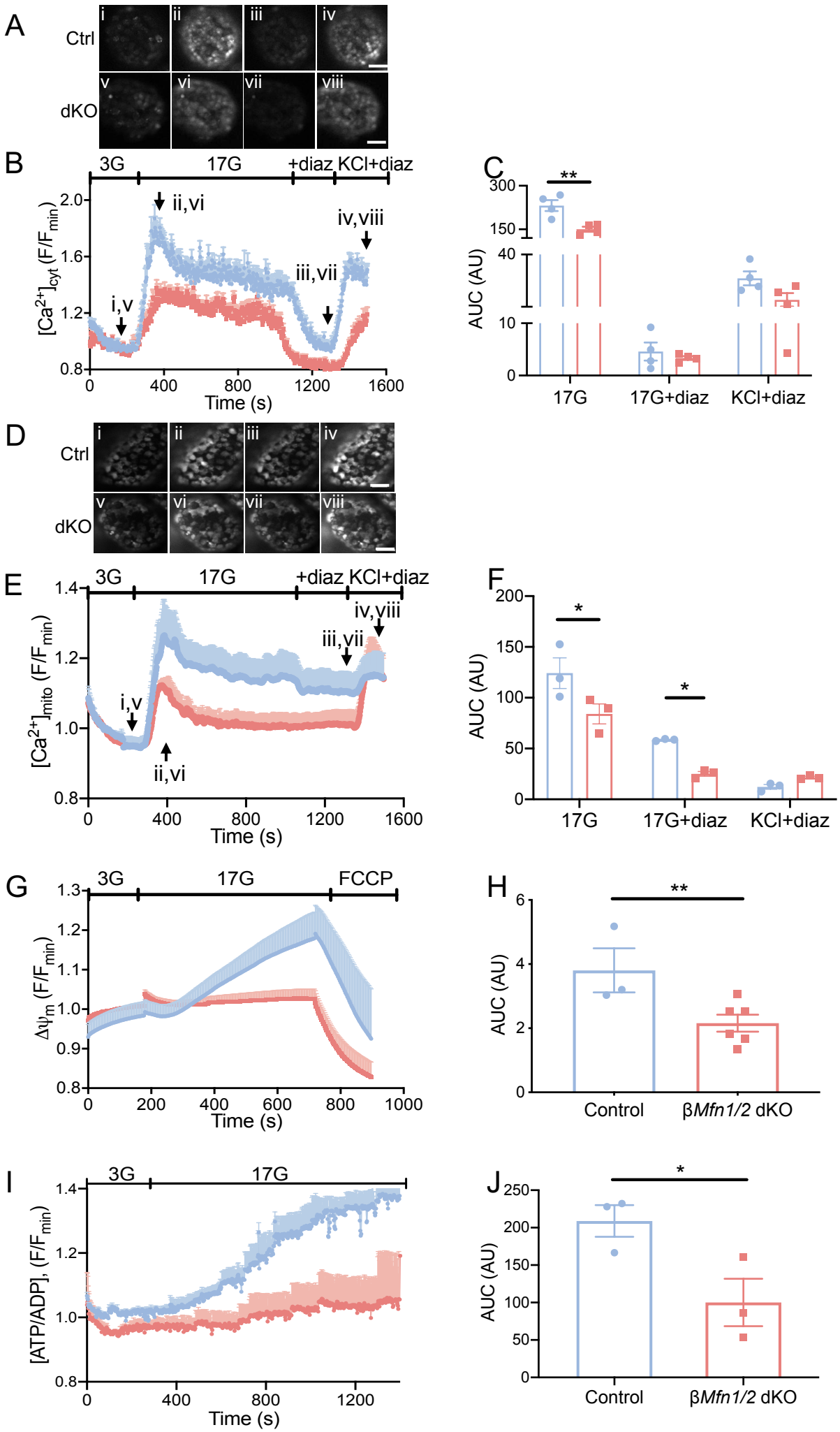
A
Ctrl
dKO
i
ii
iii
iv
v
vi
vii
viii
B
3G
17G
+diaz
KCl+diaz
ii,vi
iv,viii
iii,vii
i,v
[Ca2+]cyt (F/Fmin)
Time (s)
C
AUC (AU)
17G
17G+diaz
KCl+diaz
D
E
[Ca2+]mito (F/Fmin)
F
G
FCCP
Δψm (F/Fmin)
H
Control
βMfn1/2 dKO
I
[ATP/ADP], (F/Fmin)
J
Fig.5

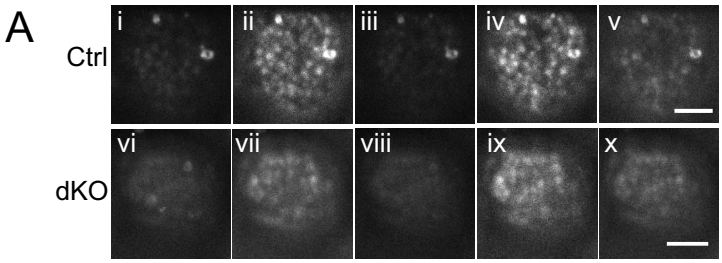
A
Ctrl
dKO
i
ii
iii
iv
v
vi
vii
viii
ix
x

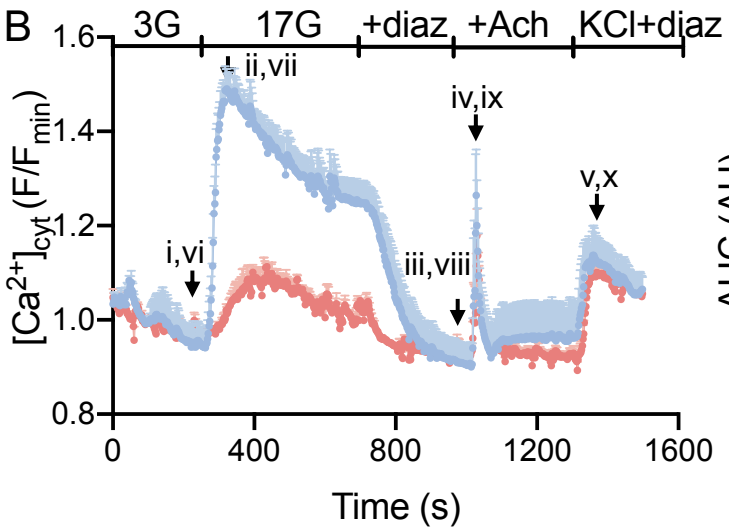
B
3G
17G
+diaz
+Ach
KCl+diaz
ii,vii
iv,ix
v,x
i,vi
iii,viii
[Ca2+]cyt (F/Fmin)
1.6
1.4
1.2
1.0
0.8
0
400
800
1200
1600
Time (s)

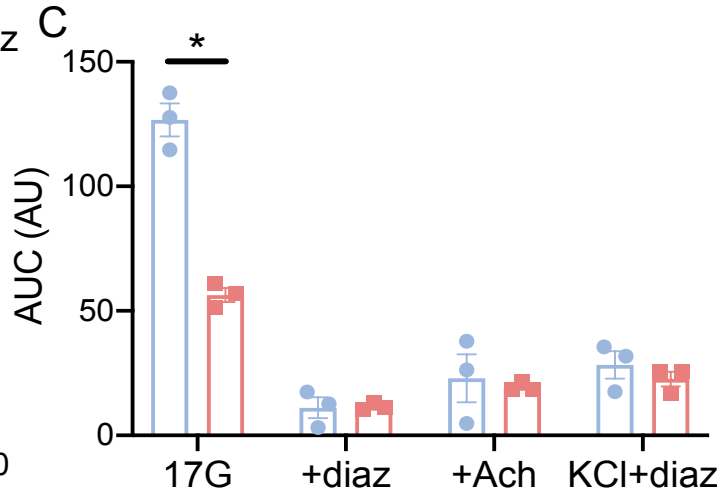
C
*
AUC (AU)
150
100
50
0
17G
+diaz
+Ach
KCl+diaz

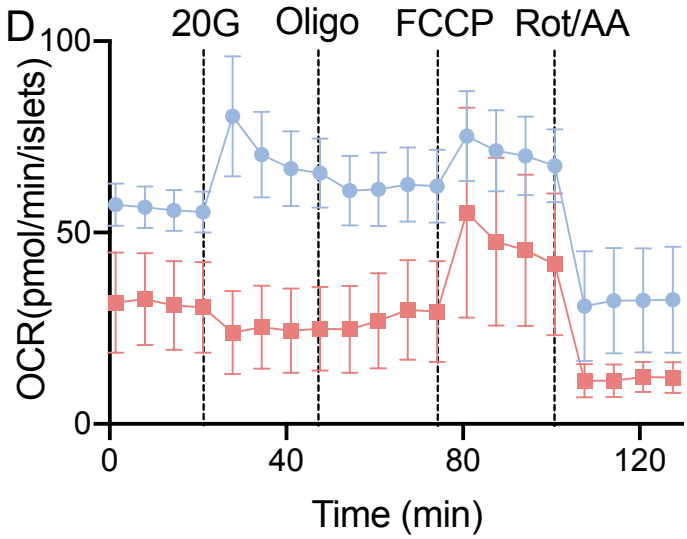
D
20G
Oligo
FCCP
Rot/AA
OCR(pmol/min/islets)
100
50
0
0
40
80
120
Time (min)

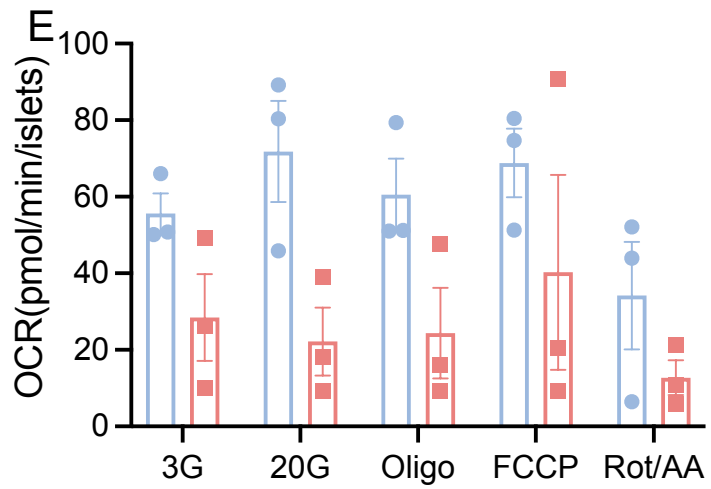
E
OCR(pmol/min/islets)
100
80
60
40
20
0
3G
20G
Oligo
FCCP
Rot/AA

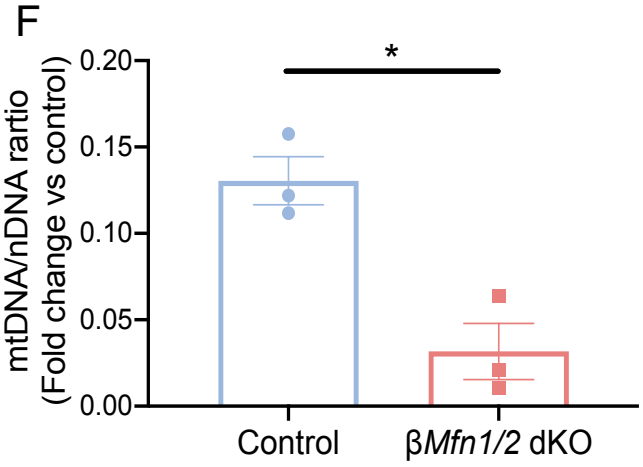
F
*
mtDNA/nDNA rartio
(Fold change vs control)
0.20
0.15
0.10
0.05
0.00
Control
βMfn1/2 dKO

Fig.6

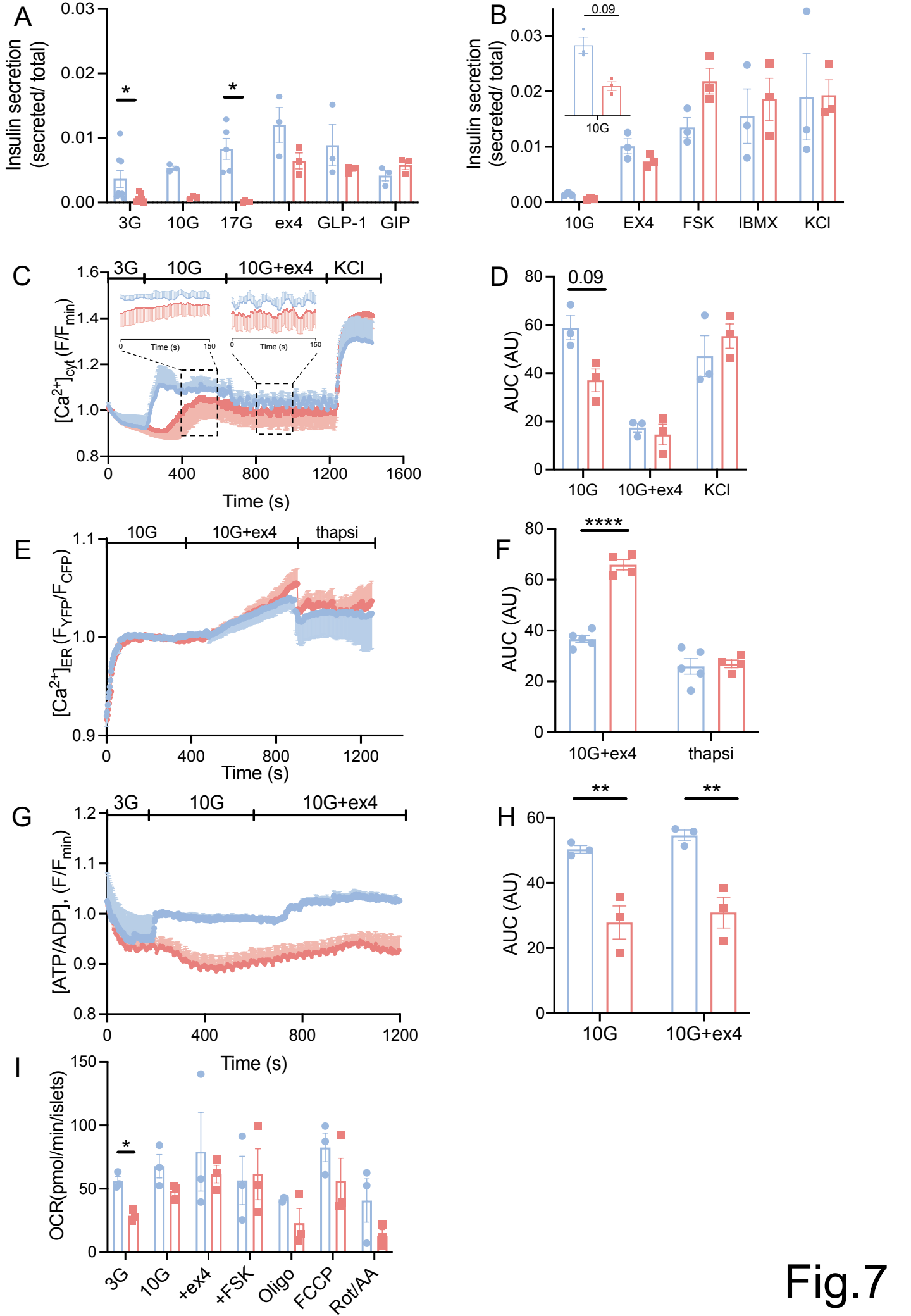
A
Insulin secretion (secreted/ total)
0.03
0.02
0.01
0.00
*
*
3G
10G
17G
ex4
GLP-1
GIP
B
0.09
10G
Insulin secretion (secreted/ total)
0.03
0.02
0.01
0.00
10G
EX4
FSK
IBMX
KCl
C
3G
10G
10G+ex4
KCl
Time (s)
150
$[Ca^{2+}]_{cyt}$ (F/F_{min})
1.6
1.4
1.2
1.0
0.8
0
400
800
1200
1600
Time (s)
D
0.09
AUC (AU)
80
60
40
20
0
10G
10G+ex4
KCl
E
10G
10G+ex4
thapsi
$[Ca^{2+}]_{ER}$ (F_{YFP}/F_{CFP})
1.1
1.0
0.9
0
400
800
1200
Time (s)
F
****
AUC (AU)
80
60
40
20
0
10G+ex4
thapsi
G
3G
10G
10G+ex4
$[ATP/ADP]$, (F/F_{min})
1.2
1.1
1.0
0.9
0.8
0
400
800
1200
Time (s)
H
**
**
AUC (AU)
60
40
20
0
10G
10G+ex4
I
Time (s)
OCR(pmol/min/islets)
150
100
50
0
*
3G
10G
+ex4
+FSK
Oligo
FCCP
Rot/AA

Fig.7

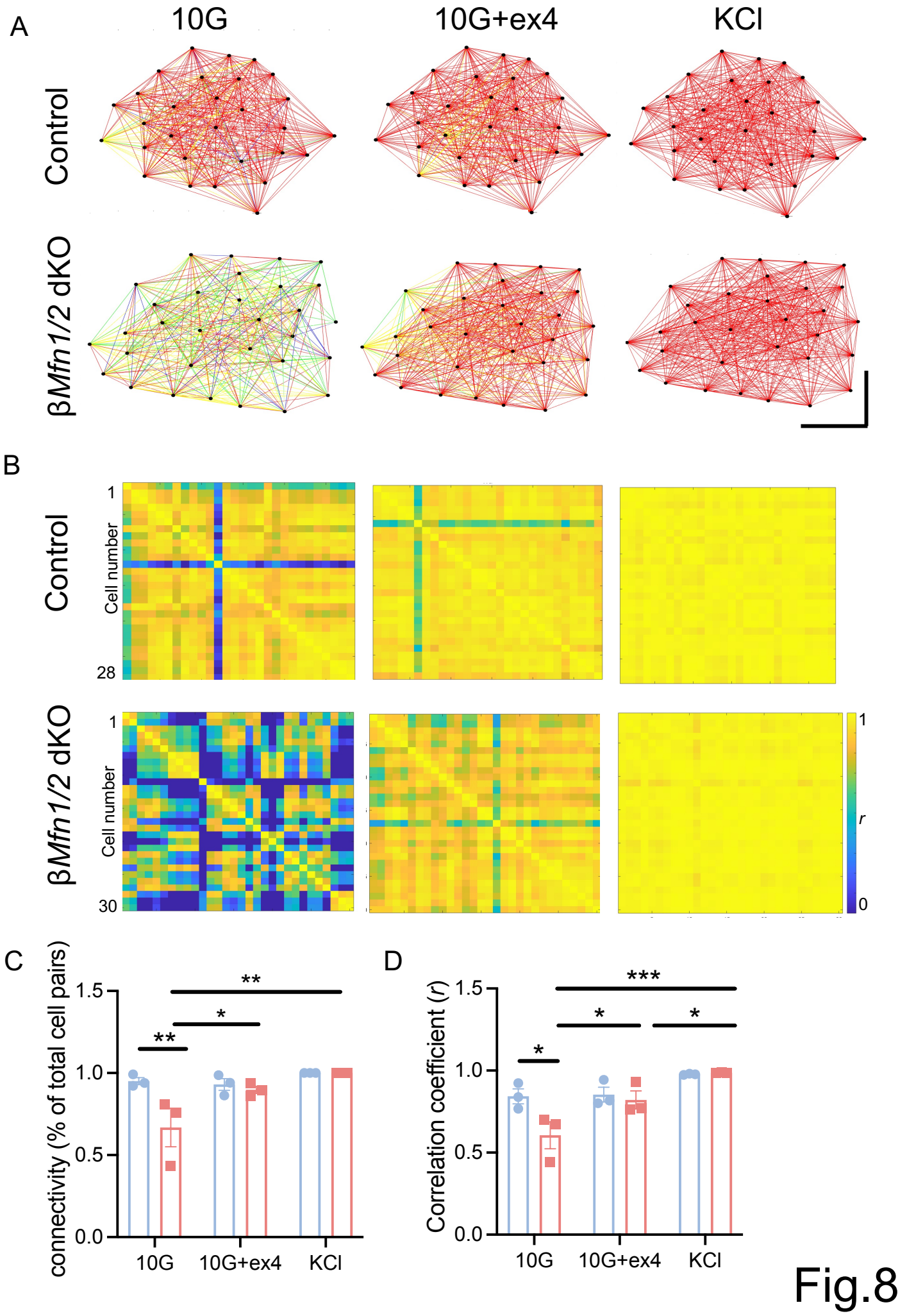
A
10G
10G+ex4
KCl
Control
βMfn1/2 dKO
B
Control
Cell number
1
28
βMfn1/2 dKO
Cell number
1
30
1
r
0
C
connectivity (% of total cell pairs)
1.5
1.0
0.5
0.0
**
*
**
10G
10G+ex4
KCl
D
Correlation coefficient (r)
1.5
1.0
0.5
0.0
***
*
*
*
10G
10G+ex4
KCl

Fig.8

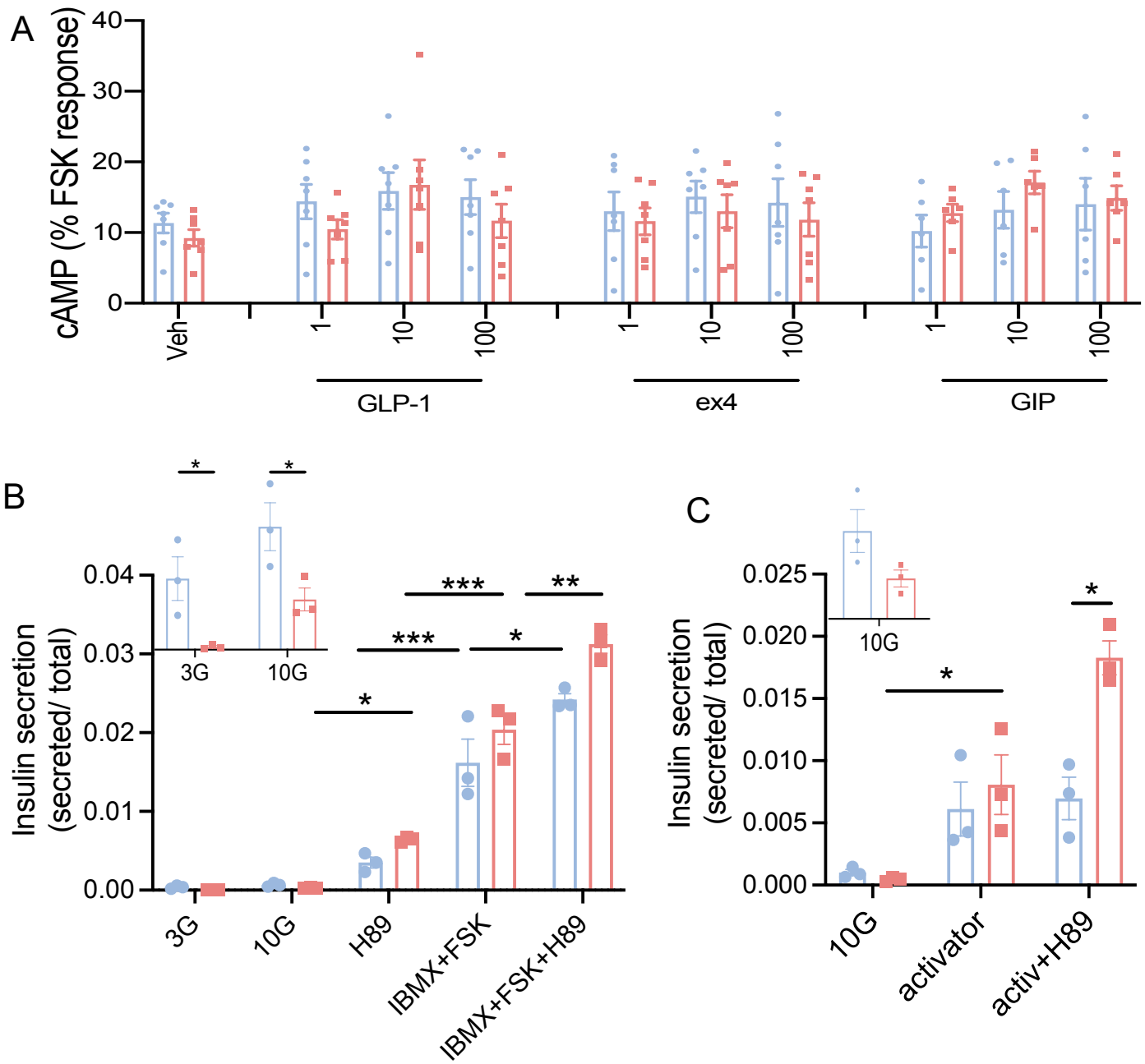
A
cAMP (% FSK response)
40
30
20
10
0
Veh
1
10
100
1
10
100
1
10
100
GLP-1
ex4
GIP
B
Insulin secretion
(secreted/ total)
0.04
0.03
0.02
0.01
0.00
3G
10G
H89
IBMX+FSK
IBMX+FSK+H89
*
***
**
C
0.025
0.020
0.015
0.010
0.005
0.000
10G
activator
activ+H89

Fig.9